Ph. D Dissertation

Study on the upper mantle discontinuities around the Korean Peninsula using teleseismic receiver functions with a CCP stacking method

원격수신함수의 CCP 합산 방법을 사용한 한반도 주변 지역의 상부 맨틀 불연속면에 관한 연구

August 2016

School of Earth and Environmental Sciences

Seoul National University

Sang-Hyun Lee

ABSTRACT

Study on the upper mantle discontinuities around the Korean Peninsula using teleseismic receiver functions with a CCP stacking method

Sang-Hyun Lee

Seismology, geophysics

School of Earth and Environmental Sciences

The Graduate School

Seoul National University

The topography of the 410 and 660 km seismic upper mantle discontinuities beneath the Korean Peninsula and southwestern Japan was determined using teleseismic receiver functions. The P receiver functions were migrated from delayed times to corresponding piercing (conversion) points of P-to-S converted phases, using one-dimensional (1-D) and three-dimensional (3-D) models. The receiver functions were then stacked using common conversion point (CCP) techniques to enhance signal-to-noise ratios to thereby reduce uncertainty (noise). The 410 and 660 km discontinuities were clearly imaged as positively valued amplitude peaks of the CCP stacked

receiver functions in the study area. The topographic variations were roughly consistent with the low temperature of the subducting Pacific Plate. However, the complex structure of the subducting Pacific Plate produced distinct changes in the upper mantle discontinuities, which cannot be explained by the temperature variations alone. The depression of the 410 km discontinuity, observed in a wide region extending from the Korean Peninsula to Kyushu Island, may be related to trench rollback history. Furthermore, the topography of the 660 km discontinuity varies significantly with latitude. At latitudes higher than 38° N, its depth remains unchanged despite the presence of the stagnant slab, while significant depression has been observed at latitudes below 36° N. This may have been caused by differences in the angles of subduction of the Japan slab and the Izu-Bonin slab. However, the heterogeneity of the water content of the slabs may also have contributed to this topographical difference.

The topography of the lithosphere-asthenosphere boundary (LAB) beneath the Korean Peninsula was determined using teleseismic S-receiver functions. The receiver functions were migrated from the delayed time to the corresponding conversion points of S-to-p phases using the IASP91 model. Signals representing the low velocity layers beneath the Korean Peninsula were imaged by applying the CCP stacking method. The LAB beneath the Korean Peninsula was imaged at a depth range of 60 - 100 km. This shallow LAB, considering the Precambrian bedrock, implied the lithosphere thinning accompanied by the coeval subduction of the paleo-Pacific plate in the

Jurassic. The distinct difference in the LAB structure across the tectonic boundary between the Gyeonggi Massif (GM) and the Okcheon Fold Belt (OFB) was recognized. The LAB at the southern part was shallower than that at the northern part. Furthermore, an additional negative discontinuity was observed below the LAB at the southern part. The structure resembles that produced by the continental collision as reported beneath Tibet. However, the continental collision had finished in the Early Triassic in the Korean Peninsula before the lithosphere thinning, which would have destroyed the lower lithosphere in the Jurassic. Therefore, the current LAB structure could not be a remnant of the continental collision. The subduction of the oceanic ridge between the Izanagi Plate and the Pacific Plate at ~60 Ma might have induced lithosphere delamination in the southern part. However, the corresponding evidence of magmatism, supporting the additional delamination in the southern part, is not reported. Unfortunately, none of existing tectonic models of the Korean Peninsula properly explain the LAB structure beneath the Korean Peninsula. Nevertheless, the presented LAB structure beneath the Korean Peninsula could contribute to establishing and understanding the tectonic history of the Korean Peninsula.

Keywords : teleseismic receiver function, CCP stacking method, the Korean Peninsula, the 410 km discontinuity (the 410), the 660 km discontinuity (the 660), lithosphere-asthenosphere boundary (LAB)

Student Number : 2002-20598

Table of Contents

List of Figures

INTRODUCTION

PLATE TECTONICS AND UPPER MANTLE DISCONTINUITIES

The outermost shell of the Earth is not stationary but is moving continuously and is composed of many plates. The rigid plates travel around the surface of Earth by floating on the ductile mantle. Some plates are subducting beneath other plates and sink into the deep mantle. Some plates are created and grow at ridges. The seismic discontinuities at the upper mantle and the mantle transition zone play important roles in understanding plate tectonics.

The 410 km and the 660 km discontinuities are observed at global average depths of 410 and 660 km, seismologically. These discontinuities play an important role in mantle convection, which is regarded as a driving force of plate tectonics. The discontinuities are formed by a phase transition from olivine to wadsleyite and ringwoodite to perovskite + magnesowüstite, respectively. They act as an accelerator of or a barrier to the subducting cold slab and the upwelling hot mantle, respectively.

The lithosphere-asthenosphere boundary (LAB) is also a key feature describing plate tectonics. The brittle lithosphere, divided into the crust and the lithospheric mantle, is floating over the ductile asthenosphere. Although

the mechanism of the formation of the LAB is not fully understood, the discontinuity is globally observed [*Schmerr*, 2012].

TECTONIC ENVIRONMENT SURROUNDING THE KOREAN PENINSULA

The Korean Peninsula is a very old craton created in the Precambrian. Since its creation, the current complex structure of the Korean Peninsula has been built through various tectonic processes. Mainly, the Korean Peninsula is regarded as an amalgam of the Sino-Korean Block and the South China Block merged by a continental collision in the Triassic. Afterward, delamination of the lithosphere accompanying massive magmatism occurred during the Mesozoic. Recently, the East Sea and the Korea Strait opened as a result of the back-arc rift system. Even now, the Korean Peninsula is affected by the convergence margin of the plates, i.e. the Pacific Plate and the Philippine Sea Plate, subducting beneath the North American Plate and the Eurasian Plate.

METHODS

RECEIVER FUNCTION

The receiver function technique is a very efficient tool for studying the discontinuities beneath seismic stations. The receiver functions represent the impedance response of the structure beneath the seismic station. In the case of the P receiver functions, the P wavelet in the vertical component and the P-to-s converted wavelets share common sources and path effects. Therefore,

the impedance of the structure below the station is obtained by deconvolving the horizontal component by the vertical component. The receiver functions are widely used to study the seismic structure below the seismic stations.

Traditionally, the receiver functions are calculated by deconvolving the radial component with the vertical component using the P phase wavelet. The resulting receiver functions are nominated as the P receiver functions. Recently, S receiver functions have been widely used, especially to study the LAB. The S receiver functions are calculated by deconvolving the vertical components with the radial components. Often, the seismograms are further rotated to the incident angle to minimize the artifacts in the receiver functions because the incident angle of the S-to-p converted phases are much larger than that of the P-to-s converted phases. In any case, the rotation of the seismogram to the great circle path is sufficient for studying the depth of the boundaries.

From the inherit characteristics of the P and S waves, the P receiver functions are used to study the fine structure; but the high amplitudes of the multiple reverberation of the surface basins and the Moho make it hard to study the LAB. Meanwhile, the S receiver functions are free from the reverberations of the shallow structure and suitable for the study of the LAB. However, the S receiver functions cannot resolve fine structure because of the low frequency characteristic of the S wave.

COMMON CONVERSION POINT STACKING METHOD

The receiver function method assumes that the incident angle of the incoming seismic wave is nearly vertical, and the receiver functions represent the structure below the station. This assumption is successful for the study of the shallow depths, for example, the structure of the crust. For the study of the deep structure, such as the upper mantle discontinuities, the receiver functions sample impedance at locations significantly far from the station. To resolve the impedance of the deep structure, the common conversion point (CCP) stacking method is frequently used.

Stacking multiple receiver functions results in reduction of the noise and enhancement of the response of the structure. The CCP stacking method intends to enhance the response of the three-dimensional (3-D) structure by stacking data corresponding to common conversion points. The relative delayed time of the receiver function is converted to the location of the conversion point, and the amplitude at each delayed time is migrated to the corresponding conversion point. The migrated amplitudes of the receiver functions are used in the stacking with a properly organized scheme of bins. All the amplitudes of the receiver functions in defined bins are averaged in this study. For a convenient display, the averaged amplitudes calculated at all depths with a common location are displayed like the conventional receiver functions. Roughly, the CCP stacked receiver functions represent the response of the structure at certain locations as a function of depth. Because the

slowness of each phase is not considered, the amplitudes do not represent the physical properties at the depths. However, discontinuities are imaged and interpretable from the polarities of the amplitudes.

RESEARCH OBJECTIVE

The Korean Peninsula, considering the complex tectonic history, is a good location for understanding the nature of plate tectonics, as the seismological discontinuities are good indicators for the study of plate tectonics. Using seismological methodology, especially the teleseismic receiver function, the structure of the discontinuities in the upper mantle can be resolved and interpreted. The discontinuities are studied by applying the CCP stacking method to the teleseismic receiver functions. According to the inherent characteristics, the P-receiver function is used for the 410 km and the 660 km discontinuities, and the S-receiver function is used for the LAB.

In Part I, the topography of the 410 and 660 km seismic discontinuities, which define the mantle transition zone, is determined using teleseismic P receiver functions with the CCP stacking technique. To assess the effect of the heterogeneity in the velocity structure, the one-dimensional (1-D) IASP91 model and 3-D model are used for the process, and the results are compared. The results are discussed with the geometry of the Pacific slab beneath Korea and southwestern Japan.

In Part II, the structure of the upper mantle, including the topography of the LAB, is imaged using teleseismic S-receiver functions with the CCP stacking technique. The resolved topography of the LAB shows a much thinner lithosphere (< 100 km) in the Korean Peninsula for the Precambrian bedrock. Distinct differences are observed across the tectonic boundary between the Gyeonggi Massif (GM) and the Okcheon Fold Belt (OFB). The relationship between the LAB structure and the tectonic history of the Korean Peninsula is discussed.

PART. I : TOPOGRAPHY OF THE 410- AND 660-KM DISCONTINUITIES BENEATH THE KOREAN PENINSULA AND SOUTHWESTERN JAPAN USING TELESEISMIC RECEIVER FUNCTIONS

This chapter has been published in Journal of Geophysical Research [*Lee et al.,* 2014] under the title ' Topography of the 410- and 660-km discontinuities beneath the Korean Peninsula and southwestern Japan using teleseismic receiver functions'

INTRODUCTION

Studying depth variations of the 410- and 660-km seismic discontinuities—hereafter referred to as the 410, and the 660, respectively—beneath the Korean Peninsula and surrounding regions is important, as it helps to increase understanding of the effects of cold slabs on upper-mantle discontinuities. The 410 and the 660 are well-established upper-mantle discontinuities, from seismological and mineral-physical perspectives. They have been detected around the globe, and generally explained by a series of phase transformations of olivine: olivine to wadsleyite (β-spinel) for the 410, and ringwoodite (γ-spinel) to perovskite + magnesiowüstite for the 660 [*Ringwood*, 1975; *Ita and Stixrude*, 1992]. The layer in between the 410 and the 660 is defined as the Mantle Transition Zone (MTZ). Inside the MTZ, another discontinuity was observed in some regions, at a nominal depth of 520 km, attributable to the phase transformation of wadsleyite to ringwoodite [*Shearer*, 1996]. Although exact depths of phase

transformations locally vary with temperature, the type of change is determined by the Clapeyron slope. The Clapeyron slope is positive for the 410 [*Morishima et al.*, 1994], indicating that it will be elevated in a cold region such as a subduction zone. However, the Clapeyron slope is negative for the 660 [*Ito and Takahashi*, 1989], indicating that it will be depressed in such a region. Although it is well known that the 660 can play a role in interrupting slabs from descending into the lower mantle [*Ringwood*, 1994], how slabs are affected in detail significantly varies from place to place.

The Pacific Plate is subducting underneath the North America (or Okhotsk) Plate at the Japan Trench, and underneath the Philippine Sea Plate at the Izu-Bonin Trench, respectively, with varying convergence rates and slopes. While the Japan slab, subducting westward at the Japan Trench, has a gentle slope and reaches a depth of 660 km beneath the eastern coast of the Korean Peninsula, the Izu-Bonin slab, subducting in southwest direction at the Izu-Bonin Trench, has a steeper slope and already reaches this depth beneath Kyushu Island, Japan [*Gudmundsson and Sambridge*, 1998] (Figure 1a). Furthermore, tomographic images of seismic high-velocity anomalies from previous studies clearly showed that the Japan and Izu-Bonin slabs penetrate the 410, while they tend to flatten out over the 660 [*Mégnin and Romanowicz*, 2000; *Huang and Zhao*, 2006]. From this, it can be inferred that these slabs are not directly descending into the lower mantle in this

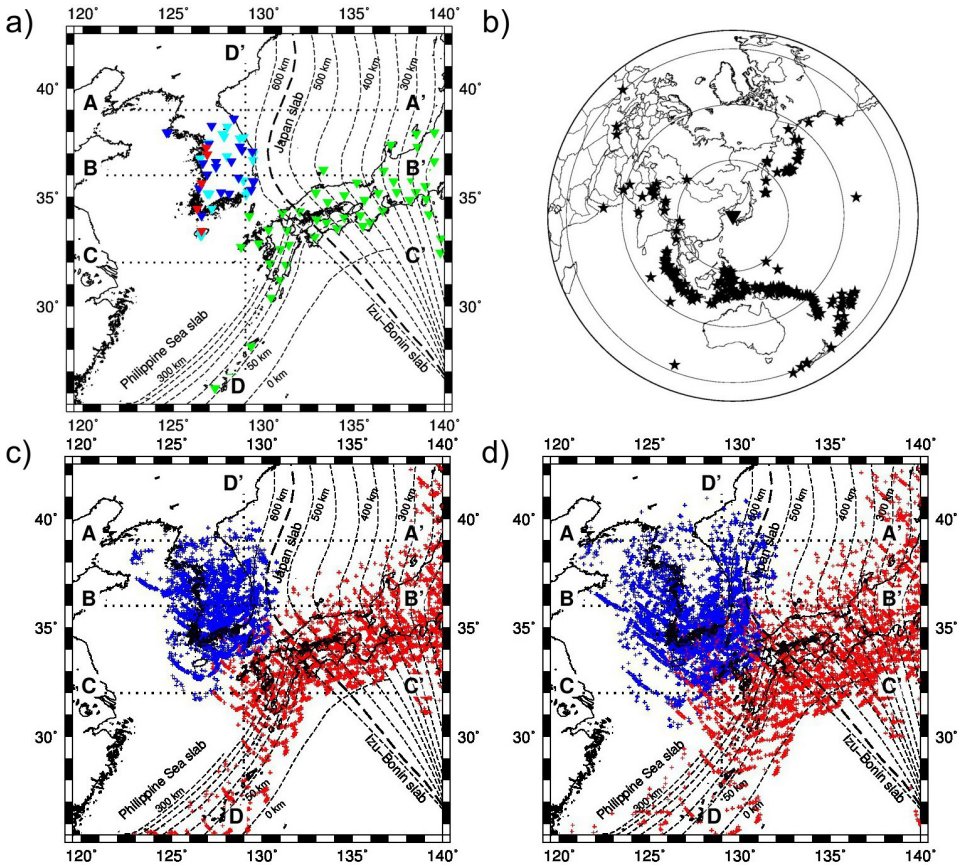

FIGURE 1. A) DISTRIBUTION OF KMA (CYAN AND RED), KIGAM (BLUE), AND FNET (GREEN) STATIONS USED IN THIS STUDY. THE DASHED CONTOUR LINES REPRESENT THE ISO-DEPTHS OF THE SUBDUCTING PACIFIC PLATE (JAPAN SLAB AND IZU-BONIN SLAB) AND PHILIPPINE SEA PLATE (PHILIPPINE SEA SLAB) WITH 50-KM INTERVALS [*GUDMUNDSSON AND SAMBRIDGE*, 1998]. THE THICK CONTOUR LINE DENOTES THE 660-LINE. DOTTED LINES (AA'–DD') ARE PROFILE LINES OF CCP STACKED RECEIVER FUNCTION SECTIONS. B) DISTRIBUTION OF EVENTS USED IN THIS STUDY, CENTERED AT (36.5°N, 128.0°E). EPICENTRAL DISTANCES OF 30°, 60°, AND 90° FROM THE CENTER ARE GIVEN BY THE CONCENTRIC CIRCLES WITH SMALLEST, INTERMEDIATE, AND LARGEST RADIUS, RESPECTIVELY. C) LOCATION OF THE CONVERSION POINTS OF P410S PHASES RECORDED AT THE KOREAN PENINSULA (BLUE) AND JAPAN ISLANDS (RED). D) SAME AS (C), BUT FOR THE P660S PHASES.

specific region. Furthermore, *Obayashi et al.* [2009] argued that the two slabs are torn apart at their junction below a depth of 300 km.

The depth variations of the 660, determined from long-period SS precursors, are in good agreement with tomographic images [*Shearer and Masters*, 1992], indicating broad depression resulting from the cold—flat-lying—slab. However, several other regional studies using receiver functions have reported otherwise. The receiver function image obtained from broadband seismic stations in Japan, and from some stations in Korea and China, shows a local depression of the 660 beneath northeast China, where the northern part of the Japan slab reaches the 660 [*Li et al.*, 2000]. Moreover, *Li and Yuan* [2003] reported similar results, recorded by a regional network of receiver functions in northeastern China. They proposed that the northern part of the Japan slab locally penetrates the 660, where slab material has accumulated. However, the spatial-sample coverage of the depressed 660 may not be sufficient, due to the limited number of stations, especially to the south. In the same region, multiple discontinuities have been reported around the depressed 660, by yet another receiver function study [*Ai et al.*, 2003]. These multiple discontinuities might be explained by phase transformations of non-olivine components in the upper mantle [e.g., *Simmons and Gurrola*, 2000], although the possibility that this discontinuity was formed by multiple reflections off shallower discontinuities of the

mantle cannot be ruled out [*Li and Yuan*, 2003].

To better understand the complex interactions between upper-mantle discontinuities and the subducting Japan slab and Izu-Bonin slab, detailed topographic maps of the 410 and the 660 beneath the Korean Peninsula and the surrounding regions are of great importance. In this study, we present for the first time, high-resolution receiver function images of the MTZ beneath the Korean Peninsula, using the Common Conversion Point (CCP) stacking method. Our image also includes the MTZ beneath southwestern Japan. Broadband seismic networks were used to produce a high-resolution receiver function image, and it complements other images obtained from previous studies for northeast China [*Li and Yuan*, 2003], east China [*Ai and Zheng*, 2003], and Japan [*Niu et al.*, 2005].

DATA AND METHODS

Broadband waveforms were obtained from the Korea National Seismic Network (KNSN), operated by the Korea Meteorological Administration (KMA), the Korea Institute of Geoscience and Mineral Resources (KIGAM), and temporary stations installed by the Korea Ocean Research and Development Institute (KORDI). The histories and instrumental information of KNSN and KIGAM network are well described in a previous study [*Park et al.*, 2010]. The KORDI temporary seismic network consists

of six stations, unevenly distributed over the western coastline of South Korea, with broadband seismometers (Guralp CMG-3T and Reftek RT 130 datalogger). We also included data recorded by F-net broadband seismic stations [*Matsumoto et al.*, 2006] in southwestern Japan, to expand our receiver function image, and to validate our results by comparison with previous receiver function results for the same region [*Niu et al.*, 2005]. The total number of stations used in this study is 123, but the number of stations used for individual events varies (Figure 1a).

We collected waveforms for 624 teleseismic events recorded by stations. To obtain a clear receiver function image, we selected events of > Mw 6.0 and epicentral distances ranging between 30°–90°. This is because waveforms can be complex due to upper-mantle triplications and P-wave diffractions along the core-mantle boundary, for epicentral distances not within this range. To avoid low signal-to-noise ratio and P-waveform complexity due to complex rupture processes, we used each waveform that had a direct P-phase signal of clear and simple shape. In total, 328 events were selected, providing a good azimuthal distribution although events with back azimuths between 0°–90° are relatively rare (Figure 1b).

Radial receiver functions were estimated by deconvolving radial components from vertical components using the iterative time-domain

deconvolution method [*Ligorria and Ammon*, 1999]. Out of the vast set of more than 13,000 receiver functions, ~5,200 receiver functions remained for further analysis, after removing noisy receiver functions. To remove noisy receiver functions, we first removed those with completeness of less than 80%. Here, completeness is defined as the cross-correlation coefficient between two radial component waveforms. One is the observed radial component waveform and the other is the predicted radial component waveform obtained by convolution of the vertical component waveform and the radial receiver function. Then, those anomalous receiver functions with highly oscillating wiggles or large low-frequency noise were manually excluded. To enhance the generally low signal-to-noise ratio of P-to-S converted phases, and thus produce clearer images of upper-mantle discontinuities, we CCP stacked receiver functions [*Owens et al.*, 2000]. For all station-event pairs, theoretical travel times and piercing (conversion) points of possible P-to-S phases were calculated for both 1D- and 3D models, at pre-defined conversion depths between 5 and 900 km, at 5-km intervals. The IASP91 [*Kennett and Engdahl*, 1991] is used as the 1D model, and the 3D model is constructed by combining the CRUST2.0 [*Bassin et al.*, 2000] and GAP-P2 [*Obayashi et al.*, 2009] models.

We migrated receiver functions from delayed times to corresponding piercing (conversion) points, by calculation of theoretical travel-time

differences between direct P waves, and P-to-S converted phases at every depth interval, enabling us to map the amplitudes of receiver functions at piercing (conversion) points of P-to-S converted phases. Two-dimensional grid cells with a lateral spacing of 0.25° were pre-defined at each depth and amplitudes of receiver functions at corresponding piercing points within 1.0° circular bins around grid points were linearly stacked. The 1.0° circular bin size was selected after testing several bin sizes. With bin sizes of 0.25º and 0.5º, coherent signals were not observed because the number of receiver functions was insufficient to suppress the noise, whereas larger bin sizes reduced the resolving power. Therefore, we decided to use the bin size of 1.0º based on considerations of stability and resolution. After CCP stacking, receiver functions could be regarded as good approximations to zero-offset data (zero source–receiver distance). Moreover, stacked amplitudes could be regarded as good approximations of the amplitudes of P-to-S converted phases at their piercing points, i.e., at the discontinuities responsible for these conversions (Figure 1c-d). To avoid distortions that occur when noise is not muted due to an insufficient number of receivers, we removed stacked amplitudes when the number of stacked receiver functions was less than 20. The depths of both the 410 and the 660 were determined by selecting the dominant peaks at corresponding depths for each grid point. In some regions, multiple peaks were observed near the depths of 410 and 660 km. However, we did not investigate these multiple peaks further. Moreover,

only dominant peaks were assumed to give reliable depth estimates of the corresponding discontinuity. However, when multiple peaks had too similar amplitudes, the dominant peak caused unstable sequences of detection, resulting in—locally—unrealistic imaging of the topography of the 410 and the 660. To reduce this effect, we applied a spatial moving average on the determined depths of the 410 and 660 for smoothing of the topography. In addition to multiple peaks, negative peaks were also observed in the vicinities of the discontinuities, especially above the 410. These negative signals could be related to partial melting at the top of the 410 [*Song et al.*, 2004]. Although the investigation of negative peaks is important to understand the nature of the discontinuities, we set aside these observations for future study and instead, focus on the topography of the 410 and 660 in this study.

RESULTS AND DISCUSSION

Figure 2 shows the CCP stacked receiver functions, along the profiles indicated in Figure 1. To emphasize the significant peaks, positive amplitudes of up to two sigma error bounds (negative side) from the mean are shaded in black. The mean and two sigma error bounds are derived from bootstrapping. To compare seismic-velocity structure and receiver function results, we overlaid P-wave velocity perturbations that were taken from the

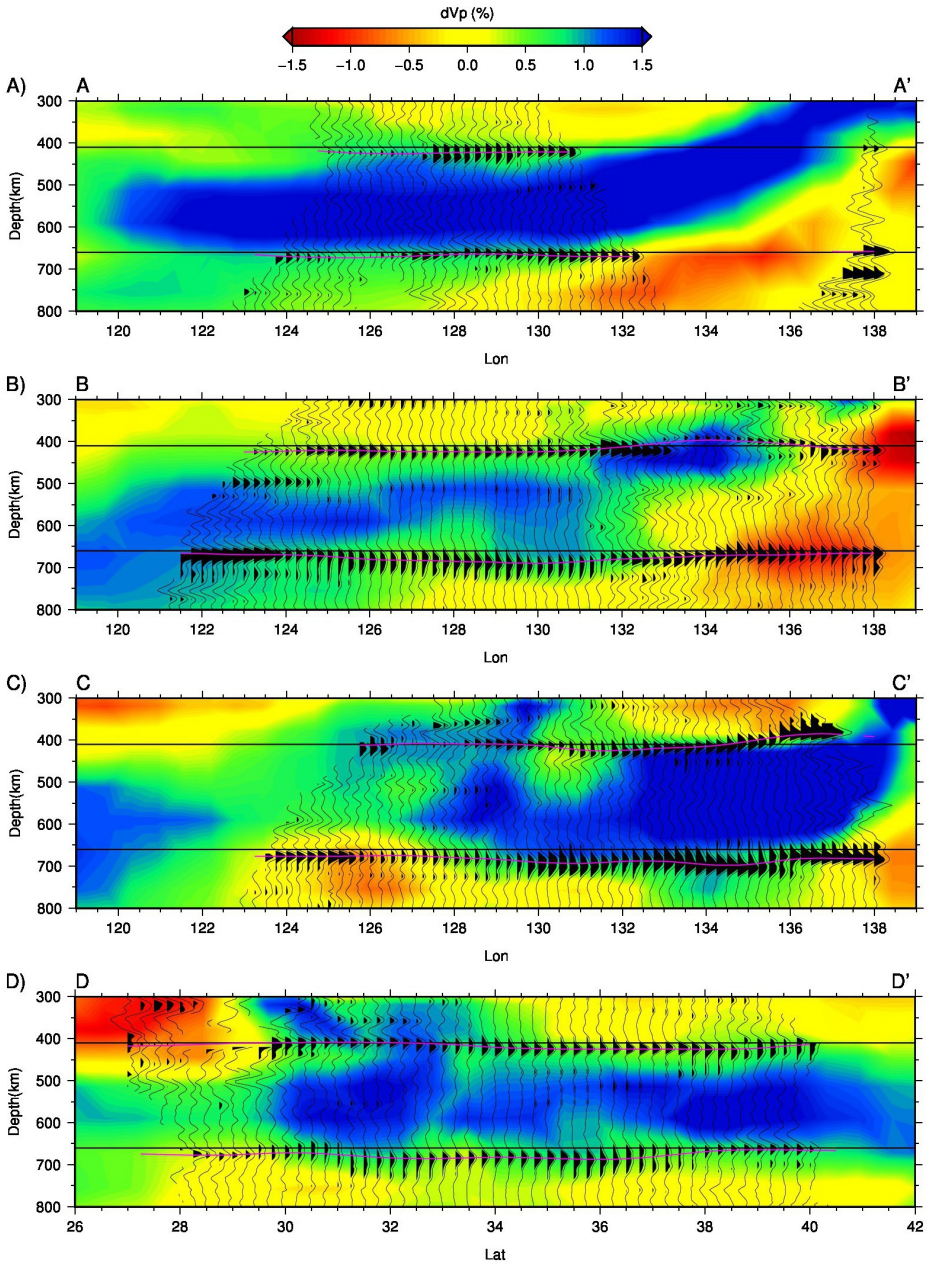

FIGURE 2. CCP STACKED RECEIVER FUNCTION SECTIONS BASED ON THE IASP91 1D-VELOCITY MODEL FOR PROFILE LINES AA'–DD'. THE POSITIVE AMPLITUDES OF UP TO TWO SIGMA ERROR BOUNDS FROM THE MEAN ARE SHADED IN BLACK. THE MEAN AND TWO SIGMA ERROR BOUNDS ARE DERIVED FROM BOOTSTRAPPING. THE BACKGROUND COLOR SPECTRUM FROM BLUE TO RED REPRESENTS FAST TO SLOW P-WAVE VELOCITY-STRUCTURE ANOMALIES, RESPECTIVELY, FROM THE GAP-P2 MODEL [*OBAYASHI ET AL.*, 2009].

GAP_P2 model [*Obayashi et al.*, 2009], on a background image. Overall, positive peaks are clearly observed at depths corresponding to the 410 and the 660. In the profiles BB' and CC' (Figure 2), the 410 is elevated where it is penetrated by the cold Pacific slab, whereas the 660 is depressed where the slab reaches a depth of 660 km. However, the topographic maps of the 410 and 660 (Figure 3a-c) show features that are more complex in terms of depth variations of the upper-mantle discontinuities. The mean depths of the 410 and 660 are 415 and 677.4 km with standard deviations of 10.3 and 9 km, respectively. Far from the subducting slab, where the velocity perturbation is not strong, the depths of the discontinuities approach global average values. Therefore, we assume that the normal depths of the discontinuities in the study area are the same as global average depths. It is widely accepted that the velocity perturbations in the tomography model represent temperature changes. Therefore, it is interesting to compare depth changes and velocity changes (Figure 3). For a more quantitative comparison, the distribution of the velocity anomaly (dVp) versus the depth change (dH) for the 410 (Figure 4b) and 660 (Figure 4d) is investigated. For the 410, it is apparent that the correlation is very poor (Figure 4b), which indicates that depth changes are not controlled primarily by temperature changes. Conversely, the theoretical linear relationship derived from the Clapeyron slope of -2.5 MPa/K explains the main trend of the distribution for the 660 reasonably well, other than for some significant scatters (Figure

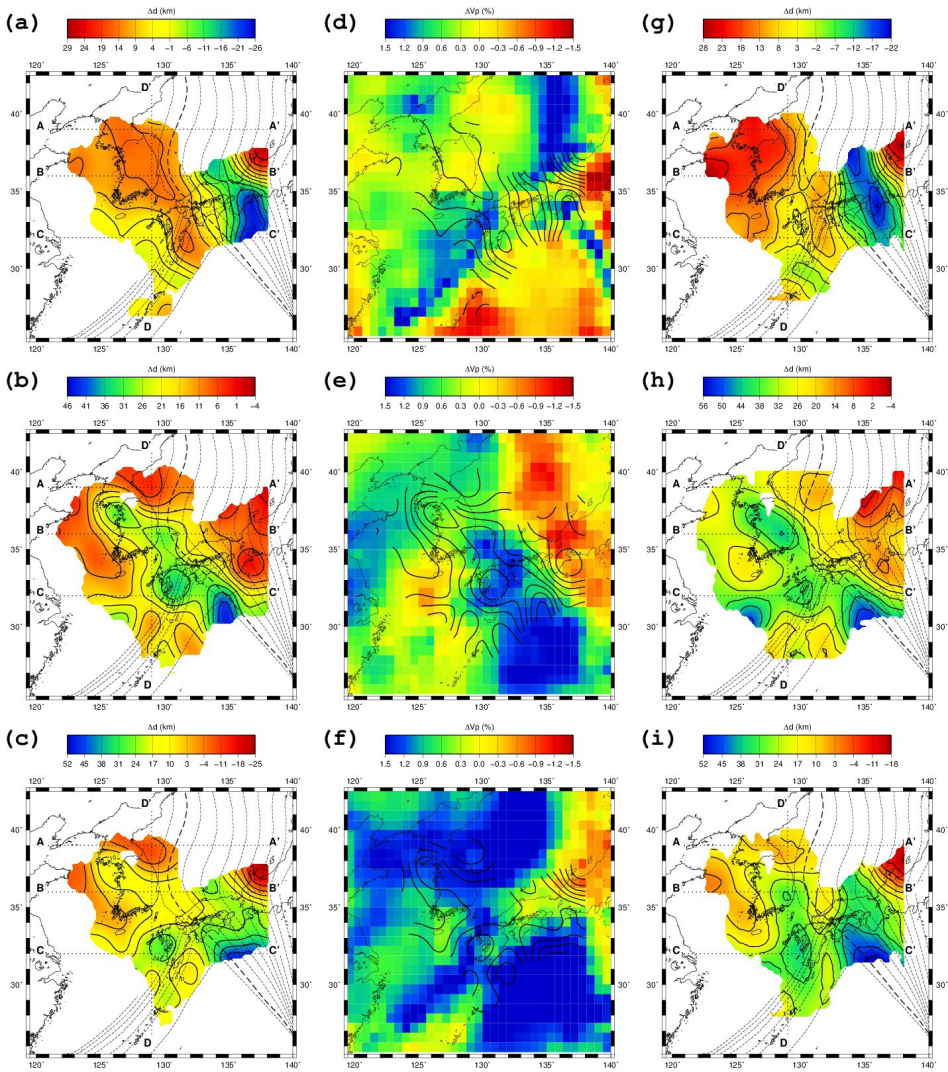

FIGURE 3. THE TOPOGRAPHY OF THE 410 (A); TOPOGRAPHY OF THE 660 (B); VARIATION OF THE MTZ THICKNESS (C) DETERMINED WITH THE IASP91 1D-VELOCITY MODEL. THE VELOCITY PERTURBATION AT THE CORRESPONDING DEPTHS TO THE 410 (D), THE 660 (E), AND THE MTZ THICKNESS (F) FROM GAP-P2 [*OBAYASHI ET AL.*, 2009] WITH CONTOUR LINES OF THE TOPOGRAPHY. THE TOPOGRAPHY OF THE 410 (G); TOPOGRAPHY OF THE 660 (H); VARIATION OF THE MTZ THICKNESS (I) DETERMINED WITH THE 3D-VELOCITY MODEL. THE COLORS REPRESENT THE PERTURBATION OF DEPTH WITH RESPECT TO 410 KM (A, G), AND TO 660 KM (B, H); OR OF THICKNESS WITH RESPECT TO 250 KM (C, I). CONTOUR LINES OF TOPOGRAPHY ARE DRAWN WITH INTERVALS OF 10 KM. OTHERS ARE THE SAME AS FIGURE 1A.

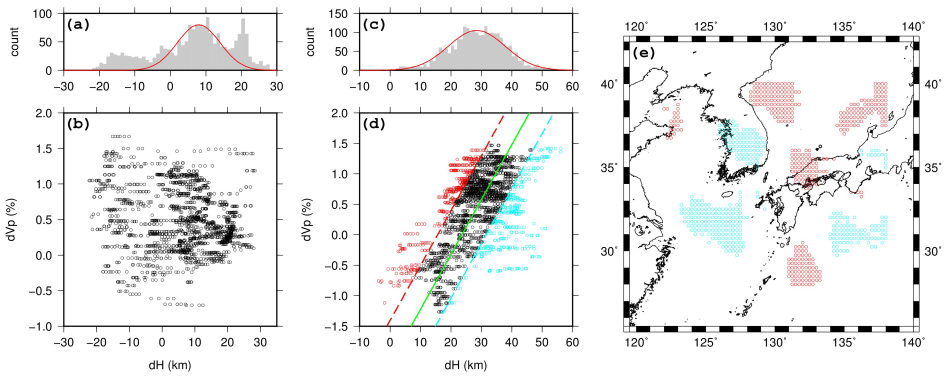

FIGURE 4. (A) HISTOGRAM OF THE DH (DEPTH VARIATION) OF THE 410 SHOWN AS GRAY BARS WITH BEST FITTING NORMAL DISTRIBUTION IN RED LINE. (B) THE DISTRIBUTION OF THE DVP VERSUS DH OF THE 410. (C AND D) SAME AS (A) AND (B), BUT FOR THE 660. THE GREEN LINE REPRESENTS THE BEST FITTING LINE WITH CLAPEYRON SLOPE OF -2.5 MPA/K AND THE DASHED LINES REPRESENT THE STANDARD DEVIATION (SIGMA) OF THE DATA DISTRIBUTION. RED AND CYAN CIRCLES INDICATE THE SCATTERS FALLING OUTSIDE OF THE +/- 1-SIGMA ERROR BOUNDS. (E) THE GEOGRAPHIC LOCATIONS OF THE SAME SCATTERS SHOWN IN (D).

4d). Significant scatters clustered in specific regions (Figure 4e), and depth changes within those regions, might require alternative explanations besides temperature changes.

The IASP91 [*Kennett and Engdahl*, 1991], i.e., the 1D reference earth model, is widely known as a good reference model for imaging the upper-mantle velocity structure. Furthermore, it has frequently been used to map amplitudes of phases to their corresponding conversion points—by using theoretically calculated arrival times—for the purpose of CCP stacking of receiver functions [e.g., *Cao and Levander*, 2010; *Tian et al.*, 2011; *Li et al.*, 2013b; *Tauzin et al.*, 2013]. However, a major drawback of this model is that it cannot account for the lateral heterogeneities of the earth. Therefore, a 3D model of the upper-mantle velocity structure was also constructed, by combining the CRUST2.0 [*Bassin et al.*, 2000] and the GAP-P2 [*Obayashi et al.*, 2009] models. By comparing results produced by the IASP91 1D model (Figure 2 and Figure 3a-c) with those produced by the 3D model (Figure 5 and Figure 3g-i), the effects of heterogeneities of the earth can be taken into account. Figure 5 shows the CCP stacked receiver functions obtained with the 3D-velocity model along profile lines AA'–DD' (Figure 1). Again, the observed depth changes of the 410 and 660 are likely to have been the result of the low temperature of the cold Pacific Plate (Figure 2). The 410 and 660 are estimated to be deeper when the 3D-velocity model is

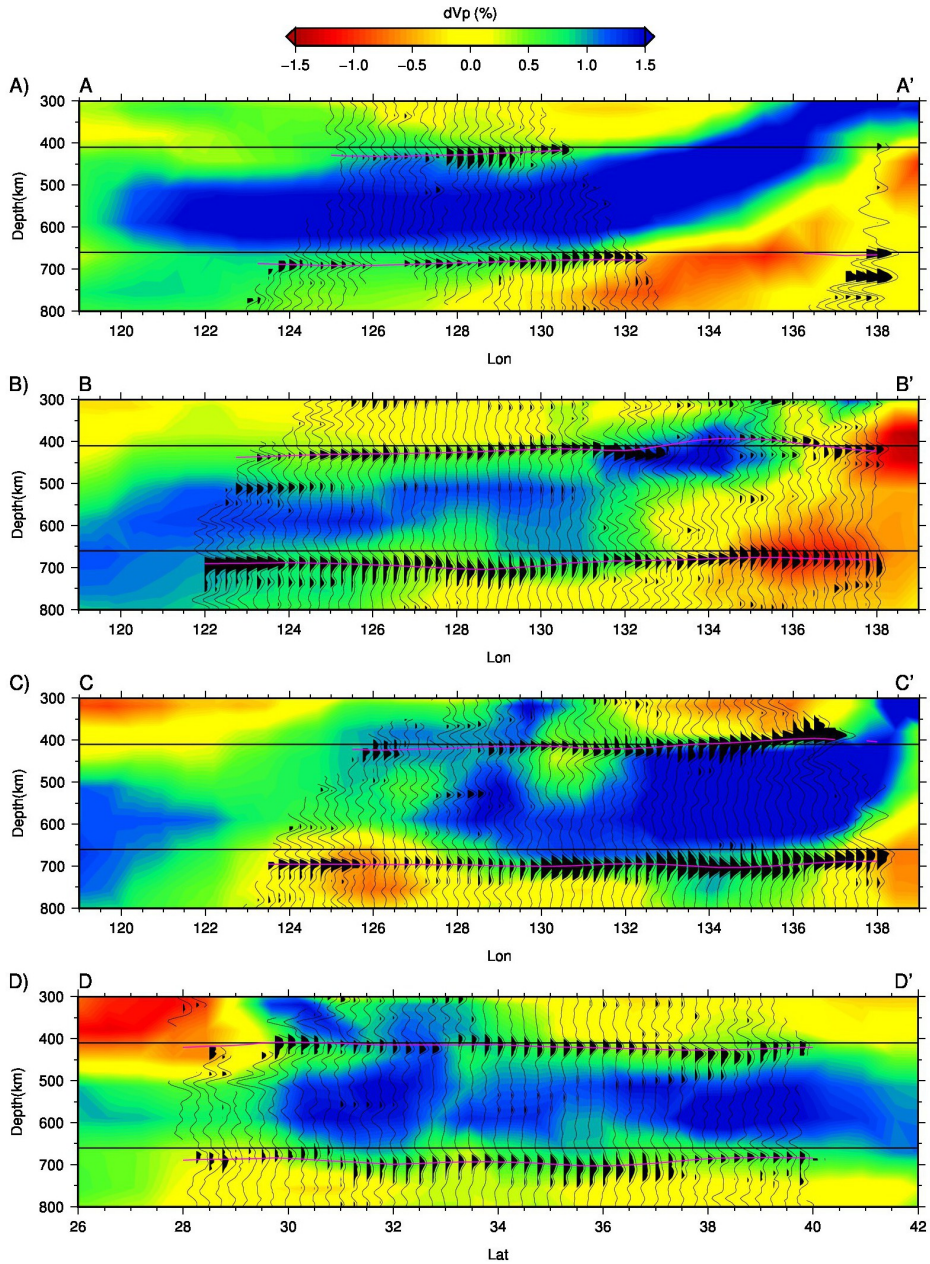

FIGURE 5. CCP STACKED RECEIVER FUNCTION SECTIONS BASED ON THE 3D-VELOCITY MODEL CONSTRUCTED FROM CRUST2.0 AND GAP-P2 FOR PROFILE LINES AA'–DD'. THE POSITIVE AMPLITUDES OF UP TO TWO SIGMA ERROR BOUNDS FROM THE MEAN ARE SHADED IN BLACK. THE MEAN AND TWO SIGMA ERROR BOUNDS ARE DERIVED FROM BOOTSTRAPPING. THE BACKGROUND COLOR SPECTRUM FROM BLUE TO RED REPRESENTS FAST TO SLOW P-WAVE VELOCITY-STRUCTURE ANOMALIES, RESPECTIVELY, FROM THE GAP-P2 MODEL [*OBAYASHI ET AL.*, 2009].

used. Differences in depths based on the 1D and 3D models become apparent in the western part of the study area. In theory, discontinuity depths—i.e., depths of P-to-S conversion points—become greater as Vp becomes higher, or as the Vp/Vs ratio becomes lower in the reference model. Compared with the IASP91 model, higher P-wave velocities (Vp) above the 410-km depth of the GAP_P2 model, can result in greater depths of both the 410 and 660. In this study, the Vp/Vs ratio is held fixed (at a value of 1.8) to facilitate construction of a 3D-velocity model. At this point it must be emphasized that recently, a higher water content was reported in the MTZ of the northwestern Pacific subduction zone [*Li et al.*, 2013a]. In the case of higher water content, a Vp/Vs ratio higher than 1.8 would be expected. Therefore, the depression of the 660 may be overestimated in this study. Figure 3g-i shows the topography of the 410 and 660 based on the 3D-velocity model, similar to Figure 3a-c.

Comparing Figure 3g-i with Figure 3a-c, the absolute depths of discontinuities are different. The difference between the topographic results obtained with the 1D and 3D models is shown in Figure 6. The difference maps for the 410 and 660 show consistent patterns. This indicates that the velocity structure above the 410 is more important for the 3D correction in this region. Although the difference between 1D and 3D corrections is not negligible, observed features in both topographic maps are generally

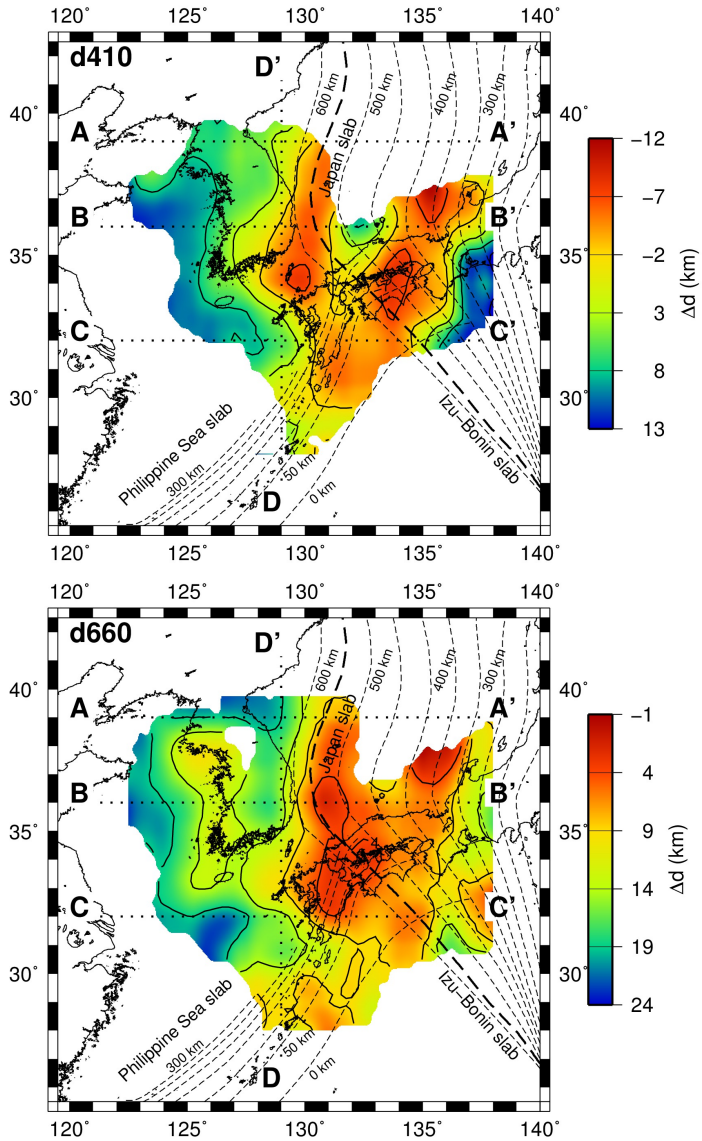

FIGURE 6. DIFFERENCES BETWEEN THE TOPOGRAPHIC RESULTS OBTAINED WITH THE 1D AND 3D MODELS FOR THE 410 (TOP) AND THE 660 (BOTTOM).

consistent regardless of the reference model. Hence, it is unlikely that the observed lateral-depth variation of the upper-mantle discontinuities has been caused by the velocity model used for migration of receiver functions.

Three major anomalous features are identified from the topography of the 410 in the study area. Firstly, an elevation of the 410 is observed where the cold subducting slab penetrates and passes through it, commonly associated with the positive Clapeyron slope of the Olivine-to-Wadsleyite transition. Many researchers have reported that the 410 beneath Japan is elevated by the effect of the cold Pacific slab [e.g., *Tono et al.*, 2005]. This elevation of the 410 has also been reported by receiver function studies [*Niu et al.*, 2005; *Tonegawa et al.*, 2005]. However, *Li et al.* [2000] did not detect the elevation of the 410, although they used a methodology identical to our own. According to *Li et al.* [2000], this could be explained by the issue of steep depth change, which could not be resolved in this narrow region of the elevated 410, due to low resolution resulting from the larger size of the stacking bin used in their study. Our results show features that are more detailed. If we look into the pattern of the elevated 410 shown in Figure 3a, the width of the elevated 410 becomes minimal—i.e., narrowest—around a latitude of 35°N, where tearing of the subducting slab has been reported by *Obayashi et al.* [2009]. This could indicate that our study has detected the gap of the torn subducting slab, where the 410 might not be elevated.

However, this feature is not clear in the topographic map produced with the 3D-velocity model, due to the limited resolution of the receiver functions, and the spatial moving average used in this study. Therefore, we cannot rule out the possibility of an artifact. To ensure detection of the gap of the torn slab, a more detailed investigation is required. While the subducting Pacific Plate penetrates the 410 and descends into the MTZ, the Philippine Sea slab—subducting at the Ryukyu Trench—was also found to either reach or penetrate the 410 by *Abdelwahed and Zhao* [2007]. From the background tomography images along the profiles CC' and DD' (Figure 2c and Figure 2d), high-velocity anomalies presumably caused by the Philippine Sea slab are observed above the 410. However, corresponding depth changes of the 410 were not observed in this study. This could imply that the Philippine Sea slab does not extend down as far as the 410, i.e., no temperature anomaly exists. However, it could also imply that the Philippine Sea slab does reach the 410, but that it is too thin and not cold enough for any changes in depth of the 410 to be observable, because of its young age.

The second anomalous feature is the significantly depressed 410 around (37°N, 138°E). This depression of the 410 is observed in both topographic maps, obtained from the 1D-velocity reference model and the 3D-velocity model. A low-velocity anomaly has been reported to exist atop this region of depression by many other tomographic studies [*Bijwaard et al.*, 1998;

Fukao et al., 2001; *Zhao*, 2004; *Obayashi et al.*, 2006]. *Zhao* [2004] performed high-resolution travel-time tomography, using both local and teleseismic events recorded by dense seismic networks on the Japanese Islands, to investigate the details of the low-velocity anomaly beneath the subducting Pacific slab. Based on the resultant high-resolution tomographic images, two possible explanations have been proposed for the anomaly. One explanation involves a local mantle-convection pattern—a hot upwelling—induced by the subducting Pacific slab. The other explanation is that the anomaly might be a trace of a small mantle plume, rising upward from the lower mantle. Unfortunately, it is unclear which of these two explanations for the anomaly is more likely to be true. Two studies that used triplicated P-waveforms [*Obayashi et al.*, 2006], and multiple ScS reverberations [*Bagley et al.*, 2009], respectively, have also been performed (in the region including the anomalous area). In both studies, a low-velocity layer was observed above the 410. However, the study that used triplicated P-waveforms reported the observation of a depressed 410, while results of the multiple-ScS-reverberation study suggested an elevated 410. Although further investigations are required to reconcile these seemingly contradicting results, the depressed 410 observed in this study seems to be consistent with that observed in the triplicated-P-waveform study.

The last anomalous feature of the 410 in the study area is the broad

depression stretching from the Korean Peninsula to Kyushu Island. The histogram for the depth of the 410 shows an interesting feature (Figure 4a). The overall histogram seems to follow the normal distribution, but there is a significant peak around the depth of 430 km. The geographic points corresponding to this depth are well correlated with the broadly depressed region. The most common explanation for this broad depression is that the temperature of this region is higher than that of surrounding regions. However, any evidence of low-velocity anomalies indicating high temperatures is not reported by tomography results [*Obayashi et al.*, 2009]. The depression of the 410 might be an artifact that originated from low-velocity anomalies at the upper mantle—i.e., shallower than 300 km—in the study area [e.g., *Fukao et al.*, 1992, 2009; *Obayashi et al.*, 2006; *Zhao et al.*, 2013], except where the subducting slab exists. These low-velocity anomalies at the upper mantle result in artificial depressions when the IASP91 1D global average model is used, which is faster than the real earth. However, the coherency of the lateral-velocity structure and 410 depression patterns has been found to be poor. Therefore, it is not likely that the depression of the 410 resulted from variations in temperature alone, or that it is merely an artifact due to shallower low-velocity anomalies. In addition to variations in temperature, variations in chemical composition could also result in depth variations of the 410. For example, Schmerr and Garnero [2007] observed a seismic discontinuity at a depth that was somewhat

deeper than the global average of the 410, extending several thousands of kilometers to the east of the Nazca slab subducting underneath the South American continent. They suggested the observed discontinuity to be the lower boundary of a hydrated lens of wadsleyite, rather than an olivine-to-wadsleyite transition boundary. Furthermore, they suggested that if it were an olivine-to-wadsleyite transition boundary, that Mg enrichment in the mantle wedge resulted in the observed depression of the 410. They also suggested that the large lateral extent—from east to west—of the depression might be related to trench-rollback history.

East of the study area (Figure 1a), the Pacific Plate subducts westward. The subduction angle is gentle at the Japan Trench, becoming steeper toward the Izu-Bonin Trench. This spatial variation in the subduction angle originates from complex trench-rollback history, including the opening of the East Sea [*Miller and Kennett*, 2006]. In Figure 3a, the width of the depressed 410 varies with latitude in a way similar to the angles of subduction. This indicates that discontinuity formation at depths below 410 km—beyond the subducting slab—by trench-rollback migration might be possible, in a way similar to that suggested by *Schmerr and Garnero* [2007]. The variation of width of the 410 with latitude is not prominently visible in the map constructed using the 3D-velocity model. However, the depression of the 410 beneath the Korean Peninsula and Kyushu Island is clearly

visible (Figure 3g).

That the Pacific slab has become stagnant after reaching the 660 has been imaged by many tomographic models [*Fukao et al.*, 2001; *Huang and Zhao*, 2006; *Obayashi et al.*, 2009]. For most regions in the study area, the cold slab could be expected to be atop the 660, except for those regions where the slab might have locally descended into the lower mantle. If we assume that the petrological and chemical compositions of the slab are uniform over the study area, temperature variations at the 660 should be the dominant cause for variations of its depth. If we only consider the effect of temperature, we might expect maximized depression where it is encountered by the slab. Furthermore, we might expect a gentle westward decrease of the level of depression, as the temperature difference between the slab and the surrounding mantle decreases [*Li et al.*, 2013a]. However, at points where the slab penetrates the 660, and descends into the lower mantle, local depressions can occur because the temperature at the center of the slab is lower than at its outer parts [*Li and Yuan*, 2003].

It is clear from Figure 2, that the 660 is considerably depressed at longitudes 130ºE and 135ºE in profile lines BB' and CC', respectively, and that these regions roughly correspond to those regions where the slab encounters it. Furthermore, the level of depression slowly decreases

westward and Figure 5 shows similar features. Although these observations are more-or-less consistent with expectations, the topographic maps of the 660 show complex features (Figure 3b and Figure 3h). Based on the assumption that the thickness of the subducting slab is about 100 km, the 550-km contour line of the slab surface roughly indicates where the slab encounters the 660 and starts to affect the depth of the 660. The thick dashed line in Figure 3 indicates the 550-km contour line, which will be referred to as the "660-line" hereafter. Since the temperature of the slab is more-or-less uniform along the 660-line, it is interesting to investigate depth variations of the 660 along the 660-line, because along such lines, other depth-affecting factors might be most easily revealed. Interestingly, the depth of the 660 shows significant variation with latitude along the 660-line. The most remarkable observation is that the depressed region of the 660 extends in the NW–SE direction along the 660-line on the southeastern part of the study area. However, depression of the 660 does not appear at latitudes above 38ºN. This pattern is consistent for both maps obtained using different reference models (Figure 3b and Figure 3h).

Southeast of the study area, depressed regions of the 660 might be expected along the 660-line because of the subducting cold Pacific slab associated with the Izu-Bonin Trench. Local maxima of depression have been observed underneath Kyushu Island and the northern Philippine Sea.

Among these maxima, the significant depression underneath the northern Philippine Sea at 31ºN, 135ºE, coincides with a high-velocity anomaly at a depth of ~660 km, reported by tomographic studies [*van der Hilst et al.*, 1991; *Fukao et al.*, 1992; *Obayashi et al.*, 2006]. Using the receiver functions obtained from Ocean Bottom Seismograph stations deployed in this area, the average depth of the 660 under the stagnant slab is reported to be 691 km [*Suetsugu et al.*, 2010]. Furthermore, the preferred 1D-velocity model for determining upper-mantle structure—identified by using P-wave triplications observed slightly south of the high-velocity anomaly—shows a depression of approx. 30 km [*Shito and Shibutani*, 2001]. However, another such 1D-velocity model constructed using P-wave triplications for a region west of the high-velocity anomaly observed in this study [*Brudzinski et al.*, 1997; *Tseng and Chen*, 2004], indicates a high-velocity layer above the 660, while there are no depth changes of the 660. Results obtained using P-wave triplications provide local characteristics of the seismic-velocity structure, where seismic phases are either refracted or reflected at discontinuities. Therefore, the different results obtained for adjacent regions indicate that the depth of the 660 fluctuates significantly beneath the stagnant slab. P-wave triplication studies have also produced various results about the 660 beneath Kyushu where the locally depressed 660 is observed in this study [*Shito and Shibutani*, 2001; *Tajima et al.*, 2009]. The variety of results from P-wave triplication studies also indicates that the depth of the 660 changes

rapidly beneath Kyushu Island, which supports the possibility of a large local depression. In our study, the depth of the 660 was observed to increase by more than 40 km at the local maximum. Under the assumption of a Clapeyron slope of -2.5 MPa/K [*Fukao et al.*, 2009], this implies that the temperature is ~650 degrees lower at this maximum, compared with the surrounding mantle. If we account for the water content as well as the Clapeyron slope, the depth change of the 660 and the seismic velocity change are converted to the thermal change and the water content change [*Suetsugu et al.*, 2006]. The maximum depression of the 660 is 44 km and the velocity perturbation at the same location is 1.4%. Thus, the thermal change of -690 K and water content change of 1.1 wt.% are derived. This difference in temperature indicates the possibility of the slab penetrating the 660 and descending into the lower mantle. This is further supported by the high-velocity anomaly observed at a depth of 756 km, through the tomographic model of *Obayashi et al.* [2009].

As was mentioned earlier, the depth of the 660 along the 660-line has local maxima to the south of the study area, elevating with increasing latitude. Furthermore, the depression of the 660 becomes less than 20 km—eventually—at latitudes above 38ºN, which is consistent with previous studies that also report weak depression beneath the east coast of the central Korean Peninsula. This region of undepressed 660 is well correlated with

one of the locations where dH is not correlated with dVp (Figure 4). *Li et al.* [2000] reported a depression of the 660 in the latitude range of 30ºN–45ºN. Meanwhile, they observed that the 660 was not depressed beneath the central part of the Korean Peninsula (refer to Figure 8c and 8d in *Li et al.* [2000]). However, they have not explained why the 660 is not depressed at these latitudes. When compared in detail, our results show different features than those of *Li et al.* [2000], due to differences in resolution. However, the undepressed 660 beneath the east coast of the Korean Peninsula was consistently revealed by both this study and by *Li et al.* [2000]. Other evidence that the 660 is not depressed is presented by *Tajima et al.* [2009], who identified the preferred seismic 1D-velocity models for determining upper-mantle structure beneath northeast Asia, by performing P-wave triplication studies. Their models consistently showed a high-velocity layer above the 660, indicating the stagnant slab from latitudes 30ºN–45ºN, along the 660-line. Furthermore, they found the 660 to be depressed at latitude 37ºN, but not between latitudes 39ºN–40ºN. According to these diverse studies, it is likely that the 660 is not depressed in the latter region. There are several possible explanations for this phenomenon, despite the presence of the cold stagnant slab.

One possible explanation is the absence of the stagnant slab in this particular area. However, this is very unlikely, because of the occurrence of

earthquakes at depths below 600 km, and because of the high-velocity anomalies that have been reportedly observed above the 660 by many independent tomographic studies.

Another explanation is given by the possibility of a different petrological or geochemical composition of the slab in this particular area [*Tajima et al.*, 2009]. *Tajima et al.* [2009] suggested a hypothetical model of a hydrous garnet-rich layer, i.e., a layer of subducted crust at the uppermost part of the slab, flowing down to the 660 at the tip and the gap of the stagnant slab. This led them to interpret the non-depressed 660 to be adjacent to the depressed 660. This model also explains the discrepancy between the depressed and undepressed 660, having in common a high-velocity layer above the 660. If this model were true, the topography should have features that show regions of depressed 660 bounded by regions of undepressed 660. However, no such features could be identified from our topographic maps.

A third possible explanation is offered by the possibility of changing water content in the slab. Recently, it has been reported that the depth of the post-spinel transformation depends on water content [*Higo et al.*, 2001; *Yamada et al.*, 2009]. According to these studies, 2.0 wt.% of water can cause the 660 to depress by about 15 km without temporal change [*Cao and Levander*, 2010]. Moreover, *Litasov et al.* [2005] revealed that the

Clapeyron slope of the post-spinel transformation varies significantly with water content. They determined the Clapeyron slope to be -0.5 MPa/K for an anhydrous mantle and -2.0 MPa/K for a hydrous mantle with 2.0 wt.% of water. Furthermore, they found that the depth of the post-spinel transformation could increase by as much as 30 km in the hydrous mantle, as opposed to only 7.5 km in the anhydrous mantle (under identical temperature conditions). According to these results, even under the condition of homogenous temperature, the 660 depth might vary with water content. Therefore, the depth variations of the 660 that occur under the conditions of homogenous temperature along the 660-line might indicate water-content heterogeneity—in the slab, or MTZ—beneath the study area. However, the origins of the differences in water content remain unclear, and studies that are more comprehensive are required to investigate this.

Lastly, the depth change of the 660 could be a consequence of differences in complex geodynamical properties, such as subduction angles, or undulation of slabs. The location where the depth of the 660 changes rapidly along the 660-line is close to the boundary between the two subducting slabs associated with the Japan Trench and the Izu-Bonin Trench (if we project the boundary at the junction of the trenches at the ocean floor to a depth of 660 km, based on the assumption that the directions of subduction are uniform). This indicates that differences in depth of the 660

might be related to the characteristics of the slabs subducting at the Japan Trench and the Izu-Bonin Trench. The Japan slab subducts with an inclination of 30º [*Miller and Kennett*, 2006] and a convergence rate of 9.2 cm/yr [*DeMets et al.*, 1994], and the Izu-Bonin slab subducts with an inclination of 45º [*Miller and Kennett*, 2006] and a convergence rate of about 6 cm/yr [*Seno et al.*, 1993]. This difference in the angle of subduction of these two slabs in the northwestern Pacific, which has been attributed to the complex trench-rollback history [*Miller and Kennett*, 2006], has also been identified by the tomographic models (Figure 2). The geometrical properties of subducting slabs descending into the MTZ are determined by their angles of subduction and their convergence rates. In general, when the subduction angle is high, slabs penetrate the 660 and descend into the lower mantle. When the subduction angle is low, slabs do not penetrate the 660, but deform and bend, prior to becoming stagnant. The Japan slab and Izu-Bonin slab are generally considered stagnant above the 660. However, their different geometrical properties could result in—locally—distinct geometries of these stagnant slabs. In turn, this could lead to depth variations of the 660 along the 660-line.

CONCLUSIONS

To understand the interactions between the subducting Pacific slab and the upper-mantle discontinuities, we investigated the topography of the 410

and 660 using teleseismic receiver functions recorded by seismic stations in the Korean Peninsula and southwestern Japan. We used 1D- and 3D-velocity models to migrate receiver functions to piercing (conversion) points of P-to-S converted phases, and CCP stacking techniques were applied to construct images of the upper-mantle discontinuities. Peaks corresponding to the 410 and 660 were observed consistently between the 1D- and 3D-velocity models used for migration of receiver functions, and clearly imaged for the entire area of study, while for some regions multiple peaks were observed. The images confirm that the regional topography of the 410 and 660 are affected by the subducting slab. Moreover, the lateral variations of the depths of both discontinuities are highly complex and cannot be explained by variations in temperature alone. In general, the 410 and 660 are elevated and depressed, respectively, where there are subducting cold slabs. The region of depressed 410 observed beneath the Korean Peninsula and southwestern Japan might indicate a type of relict structure related to the complex trench-rollback history of the region. For the 660, it is well known that the slab becomes stagnant in this region. However, a considerable depression of the 660 is locally observed in the northern Philippine Sea, which might indicate that the subducting slab could penetrate the 660 and descend toward the lower mantle at certain locations. The most important finding of this study is that the depth of the 660 varies systematically along the trench axis. Possibly, this is simply because the

angle of subduction varies with latitude, although the spatial heterogeneity of water content of the slabs might also contribute to this effect. It is an interesting hypothesis, but we still need to explain how water content could be heterogeneous at this depth.

PART II: LAB BENEATH THE KOREAN PENINSULA IMAGED BY S RECEIVER FUNCTIONS

INTRODUCTION

The Korean Peninsula, located at the eastern margin of the Eurasian Plate, has undergone a complex tectonic history. The Korean Peninsula was formed by the continental collision between the Sino-Korean Block (SKB) and the South China Block (SCB) in the Permian. Since the continental collision, the Korean Peninsula has been at the plate margin. From the Jurassic, the paleo-Pacific plate (i.e., Izanagi Plate) started to subduct under the Eurasian Plate from the southeast and diminished below the Eurasian Plate around 60 Ma. Subsequently, the Pacific Plate started subducting beneath the Korean Peninsula, continuing until now.

The lithosphere-asthenosphere boundary (LAB) is a very important key to understanding the tectonic process although the mechanism of the LAB has not been fully understood. There has been no previous study about the direct local measurement of the LAB depth beneath the Korean peninsula. Some global and regional studies show LAB depths of about 85 – 100 km around the Korean Peninsula [*Artemieva and Mooney*, 2001; *An and Shi*, 2006; *Artemieva*, 2006; *Pandey et al.*, 2014]. In addition, an LAB around 70 km in depth was reported by some studies using the S receiver functions in northeastern and eastern China [*Sodoudi et al.*, 2006; *Kind et al.*, 2012].

The base rock of the Korean Peninsula was created in the Precambrian. The thickness of the lithosphere resolved from global surface wave tomography is too thin for the Precambrian craton. This thin asthenosphere is also observed in eastern China at the east of the North-South Gravity Lineament (NSGL). The thin lithosphere in the Korean Peninsula and eastern China is considered to be the result of lithosphere thinning during the Jurassic and the Cretaceous, respectively. Several models have been proposed to explain the process of the lithosphere thinning. For the most part, they are sorted into two groups by principle concepts. One group is the lithosphere delamination in which the eclogite developed by high pressure during the continental collision at the lower crust is delaminated into the deep asthenosphere. The surrounding asthenosphere is upwelled into the opened space by the delamination and a new lithosphere mantle is formed. The other group is lithosphere erosion in which the lower part of the lithosphere mantle is eroded by upwelling hot mantle. In the both cases, the mantle upwelling plays an important role in lithosphere thinning and accompanies massive magmatism or volcanism. The characteristics of the magmatism are used to discover the tectonic history.

We used an S receiver function (SRF) technique to obtain the topography of the LAB beneath the Korean Peninsula. The receiver function technique is widely used to detect the properties of the boundaries beneath the seismic stations. The S receiver function is effective in detecting the LAB because the S

receiver function is free from the reverberations developed by the shallower discontinuities, such as at the Moho and the sedimentary basins, which contaminates the response of the LAB in the P receiver functions (PRF). The common conversion point (CCP) stacking method is applied to obtain the three-dimensional structure of the seismic discontinuities.

DATA AND METHODS

Seismograms recorded by seismic stations installed on the Korean Peninsula from 2005 to 2012 are obtained (Figure 7). The distribution of the stations is shown in Figure 8. These stations are operated by the Korea Meteorological Administration (KMA) and Korean Institute of Geology and Mining (KIGAM). Events with magnitude equal to or larger than 5.5 epicentral distances within 60° - 85° are selected from EHB bulletins [*International Seismological Centre, EHB Bulletin, http://www.isc.ac.uk, Internatl. Seis. Cent., Thatcham, United Kingdom, 2009*].

Data with low signal-to-noise ratio (SNR) is excluded when calculating SRF. The SRFs are calculated for data with the SNR of the S phase greater than three. The time domain iterative deconvolution method is used to calculate SRFs [*Ligorria and Ammon*, 1999]. In the deconvolution, seismograms for 60 s before and after the theoretical arrival time of the S-phase are used. The

FIGURE 7. DISTRIBUTION OF EARTHQUAKES.

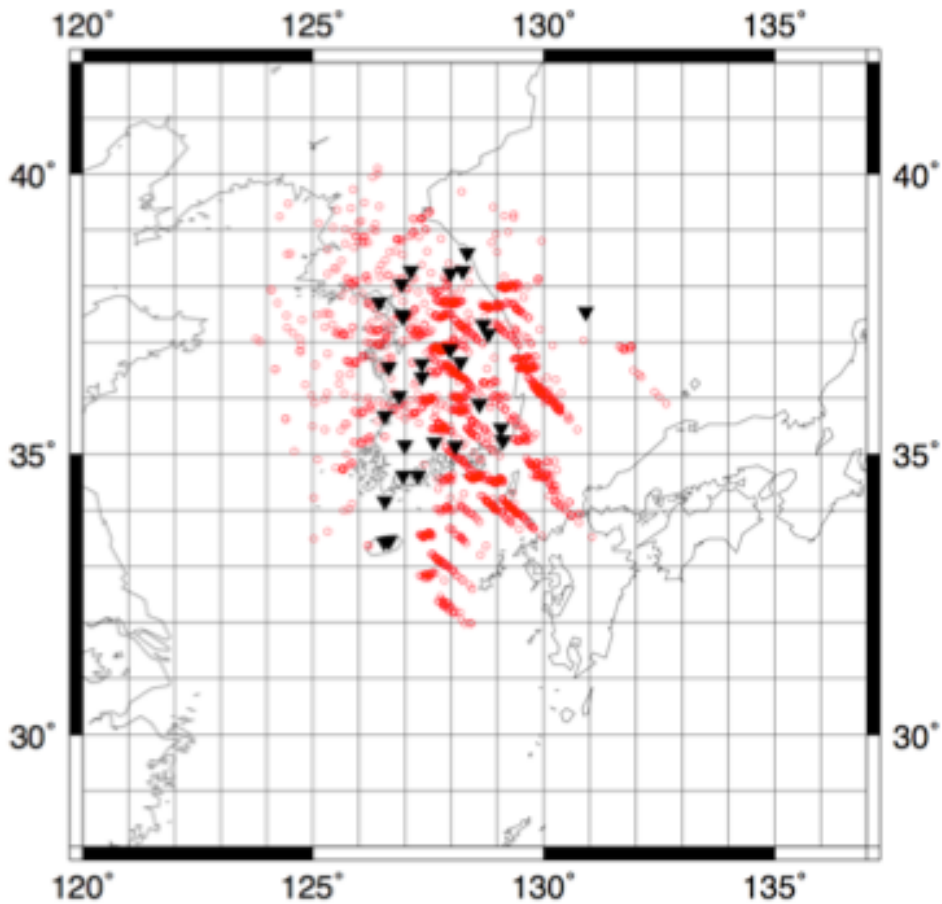

FIGURE 8. DISTRIBUTION OF THE STATIONS (TRIANGLES) AND THE CONVERSION POINTS (CIRCLES) OF THE S-TO-P PHASES AT THE 100 KM DEPTH CALCULATED WITH THE IASP91 MODEL.

horizontal components are rotated to the great circle path to evolve radial and transverse components. Because the S-to-p converted phases arrive before the S-phase, the seismograms are reversed in time. Receiver functions are obtained by deconvolving the vertical component by the radial component. The amplitudes of the receiver functions are inverted for consistency with the PRFs. Therefore, the positive signal represents the converted waves corresponding to the discontinuity of the downward velocity increase (such as Moho) and the negative signal represents those of the downward velocity reduction (such as LAB).

The length of the S-phase is different for each event. The SRFs are calculated for the data cut at several times after the S-phase arrival time. Among those SRFs obtained with various time windows, the SRF with maximum fitness is selected. The SRFs with fitness smaller than 80 are excluded. Finally, fair SRFs are selected by manual inspection at each station with some criteria. The SRFs with clear and consistent signals for the onset of Moho and those without low frequency energy are selected.

In total, 1771 SRFs were selected and used to image the discontinuities. The locations of the earthquakes of the SRFs are shown in Figure 7. The S-to-p conversion points at 100 km depth are plotted in Figure 9. The conversion points cover the Korean Peninsula in a roughly uniform pattern. The calculated SRFs are shown in Figure 10. The S-to-p converted phases at the Moho is observed at less than 5 s. Around 55 s, the S-to-p converted phases at

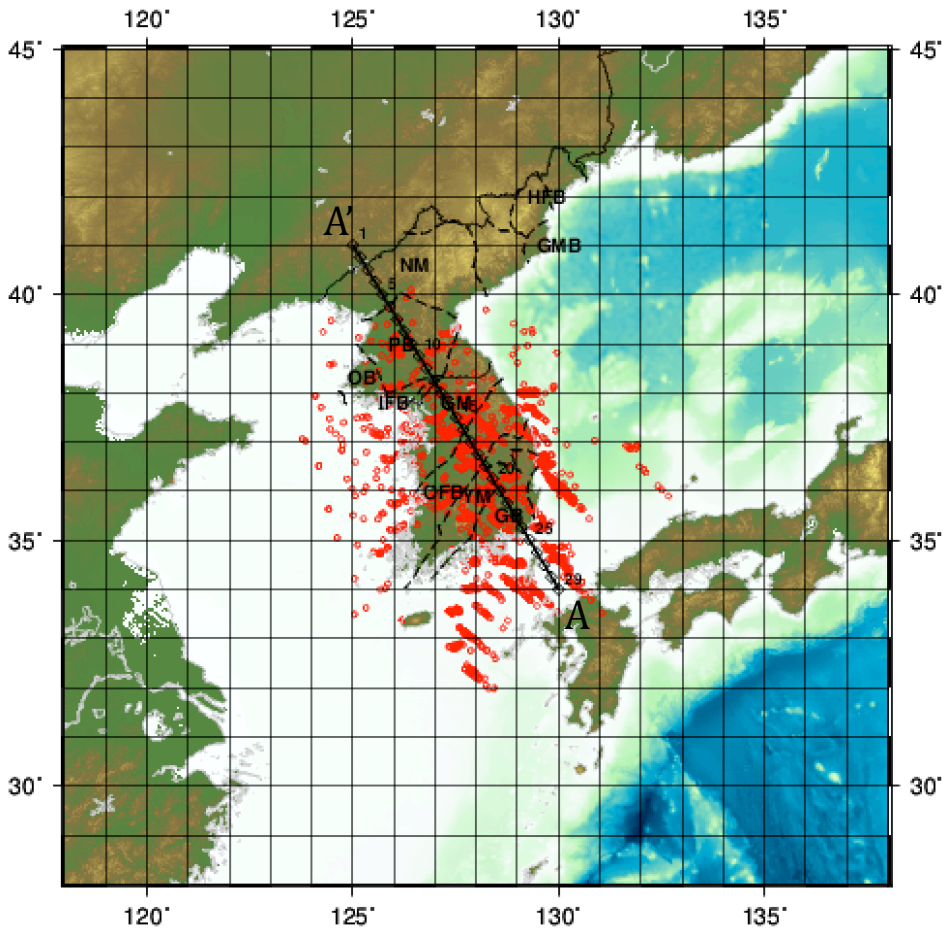

FIGURE 9. PROFILE LINE AA' FOR FIGURE 11.

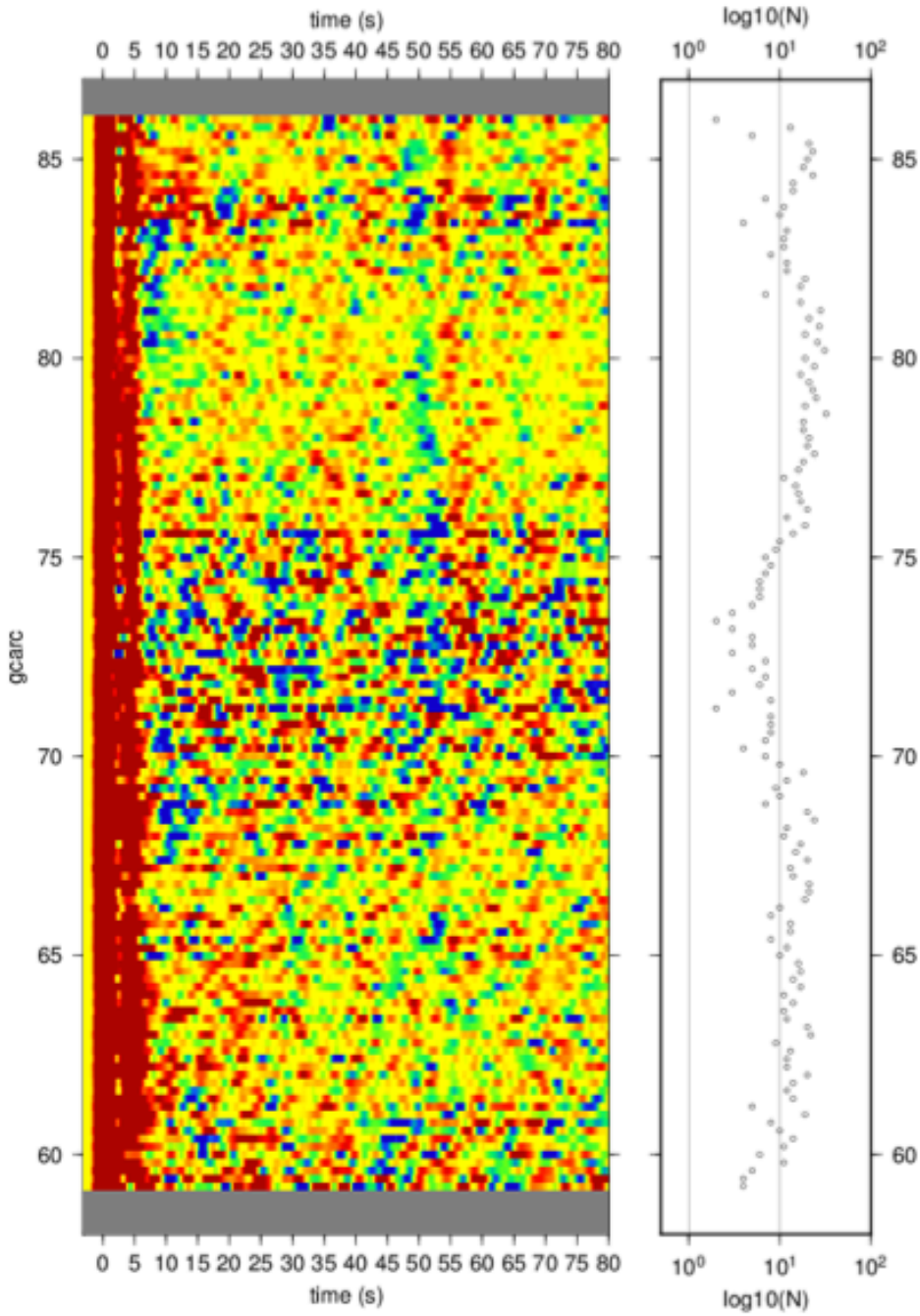

FIGURE 10. OBTAINED S RECEIVER FUNCTIONS. S RECEIVER FUNCTIONS ARE BINNED WITH AN EPICENTRAL DISTANCE OF A 1° WINDOW. THE NUMBER OF S RECEIVER FUNCTIONS THAT FALL IN EACH BIN IS PLOTTED IN THE RIGHT.

the 410 km discontinuity and the low velocity layer atop the 410 km discontinuity are recognized with epicentral distances greater than 70°.

The CCP stacking method is applied to image the LAB beneath the Korean Peninsula from the SRFs. Individual SRFs are migrated by converting the time to three-dimensional (3-D) conversion points. The time from the S-phase arrival is converted to the corresponding location of the S-to-p conversion by modeling the theoretical arrival times of conversion phases at each depth with respect to the IASP91 earth model [*Kennett and Engdahl*, 1991]. Because the theoretical conversion points are not strongly affected by the heterogeneity of the velocity model used for migration at the target depth shallower than 200 km, the use of a global average model is sufficient for the purpose of imaging the LAB. Therefore, each SRF trace is projected along the corresponding S-to-p conversion points at each depth. The projected traces in 3-D space are averaged with horizontal circular bins. The data projected on the bin are averaged. At each depth with 1 km spacing, the average amplitude is calculated using a circular bin. The size of the bin is selected to be 1.5° in radius. According to a test of various bin sizes (from 0.5° to 2° in radius), a smaller bin makes the result unstable, and a larger bin suppresses local changes.

The S-to-p phase is strongly noisy because it is contaminated by the coda of the P-phase. The S-phase itself is complex compared to the P-phase. Therefore, a noisy SRF cannot be avoided. It cannot be guaranteed that the

noise in the SRF is sufficiently suppressed through CCP stacking. To access the reality of the signals shown in the stacked receiver functions, a bootstrap test is applied. Through 300 iterations of the bootstrap test, the standard error (SE) is calculated for each bin. The SE is used to assess the robustness of the spikes in the CCP stacked images.

RESULTS

Figure 11 shows the CCP stacked SRFs obtained along the profile line AA' (Figure 9). The profile line AA', which penetrates the Korean Peninsula in the NW-SE direction, is adequate for investigating the main variation of the LAB because it is roughly perpendicular to the main extended direction of the tectonic regions. In Figure 11, the solid lines represent the stacked SRFs at each point on the profile line AA'. The positive and negative amplitudes exceeding the standard error (±1σ) of the bootstrap test are presented as areas shaded in red and blue, respectively. The blue signals represent the interfaces of the downward velocity reduction.

In the stacked SRF section along the profile line AA' (Figure 11), the stacked SRFs to the north of 39° N are large in amplitude and strongly oscillating. Furthermore, the amplitude of the SRF is smaller than the 1σ of the bootstrap test at all depths. This implies that the data is not sufficient to suppress the noise in the SRF to the north of 39° N. In other locations to the south of 39° N, robust signals are obtained by stacking the SRFs. Laterally

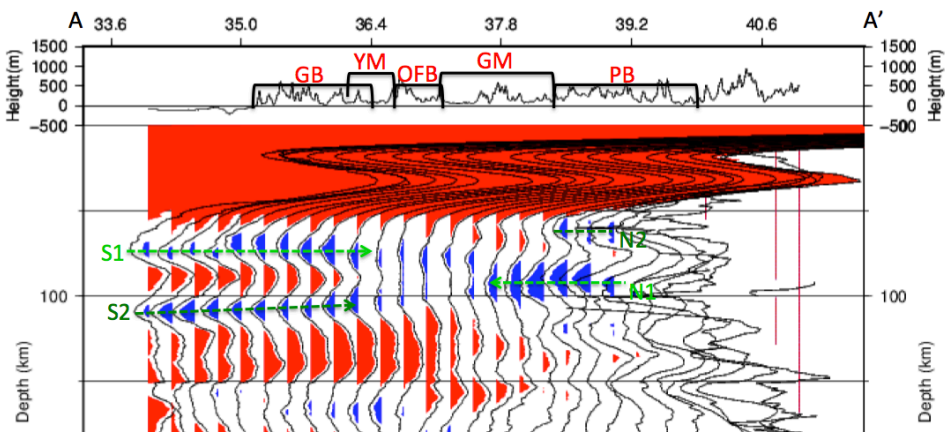

FIGURE 11. COMMON CONVERSION POINT (CCP) STACKED S RECEIVER FUNCTIONS (SRF) ALONG THE PROFILE LINE SHOWN IN FIGURE 9.

continuous signals are imaged even when 2σ of the bootstrap test is evaluated. Robust negative phases are imaged at a depth range of 50 - 120 km.

Along the profile line AA' (Figure 9), strong positive signals appear at ~35 km depth. This phase is interpreted as the SmP phase, which is converted at the Moho. This Moho depth is comparable with those of previous studies in the Korean Peninsula [*Chang and Baag*, 2007; *Yoo et al.*, 2007]. Because the target of this study is the imaging of the LAB, the details of the Moho will not be analyzed further. With the lower frequency content of the S-wave, the resolution of the SRF is lower than the PRF. Therefore, the PRF is more appropriate to study the Moho.

In the section of the stacked SRFs along the profile line AA', negative signals appear at the depth range of 50 - 120 km (Figure 11). North of ~38° N, the negative phase (labeled as N1) with an average depth of 95 km is observed. Two negative phases are observed to the south of 36° N with an average depth of 75 km (labeled as S1) and 110 km (labeled as S2). In the transition zone at the center area from 36° N to 39° N, the negative phases appear showing a branching shape from the N1 to the S1 and the S2. The S1 is consistently observed beneath the entire area with lateral continuity even when the 2σ of the bootstrap test is considered, while the S2 is not consistent (Figure 12). Therefore, the S1 and the N1 are regarded as the phases representing the LAB beneath the study area.

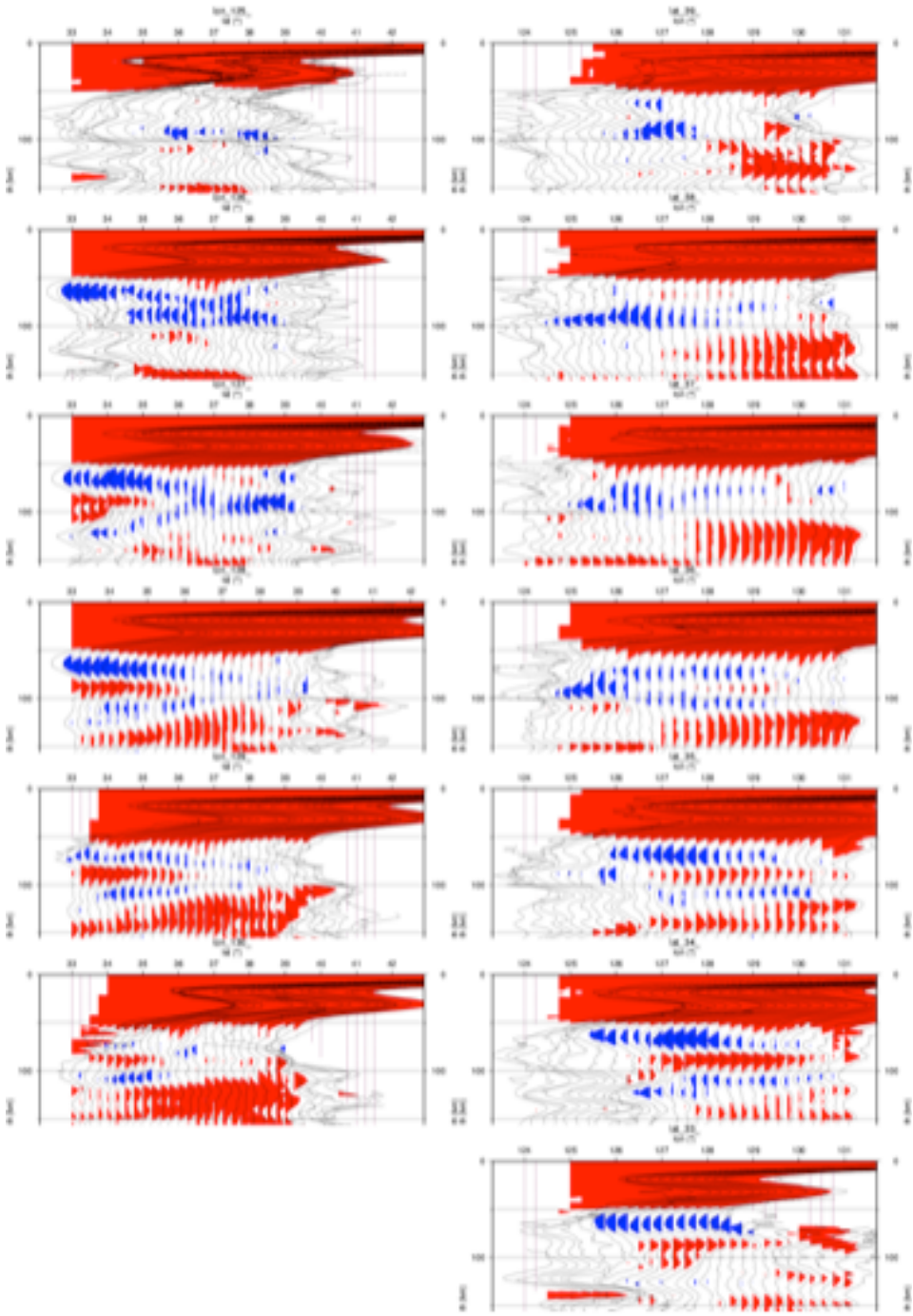

FIGURE 12. SECTIONS OF THE COMMON CONVERSION POINT (CCP) STACKED S RECEIVER FUNCTIONS (SRFS) ALONG THE LONGITUDES AND LATITUDES. THE AREAS WITH AMPLITUDES WITH 65% CONFIDENCE LEVEL ARE COLORED IN RED AND BLUE FOR THE POSITIVE AND THE NEGATIVE SIGNALS, RESPECTIVELY.

To determine the horizontal variation of the LAB depth, the CCP stacked SRFs are calculated at each point with 0.25° spacing (Figure 12 and Figure 13). The horizontal variation of the LAB depth is shown in Figure 14. The depth of the LAB is determined from each CCP stacked SRFs obtained at each grid point with spacing of 0.25°. As shown in the AA' section (Figure 11), the depth of the LAB is decreasing from north-west to south-east, and the iso-depth lines of the LAB are sub-parallel to the tectonic lines. A rapid change of the LAB depth is recognized along the western coast to the south of 37° N. This rapid change in the LAB depth extends north-eastwards from ~36° N across the Korean Peninsula. This is roughly consistent with the tectonic boundary between the Gyeonggi Massif (GM) and the Okcheon Fold Belt (OFB).

To access the uncertainty in the LAB depth determination, the thickness of the signal with amplitudes larger than 20 % of the maximum amplitude are analyzed (Figure 15). The large thickness appears where the multiple signals are merged. Figure 16 shows the analyzed uncertainty with the LAB topography. The darker area means the possibility of a larger uncertainty in the LAB depth estimation. The uncertainty increases where the LAB depth changes rapidly.

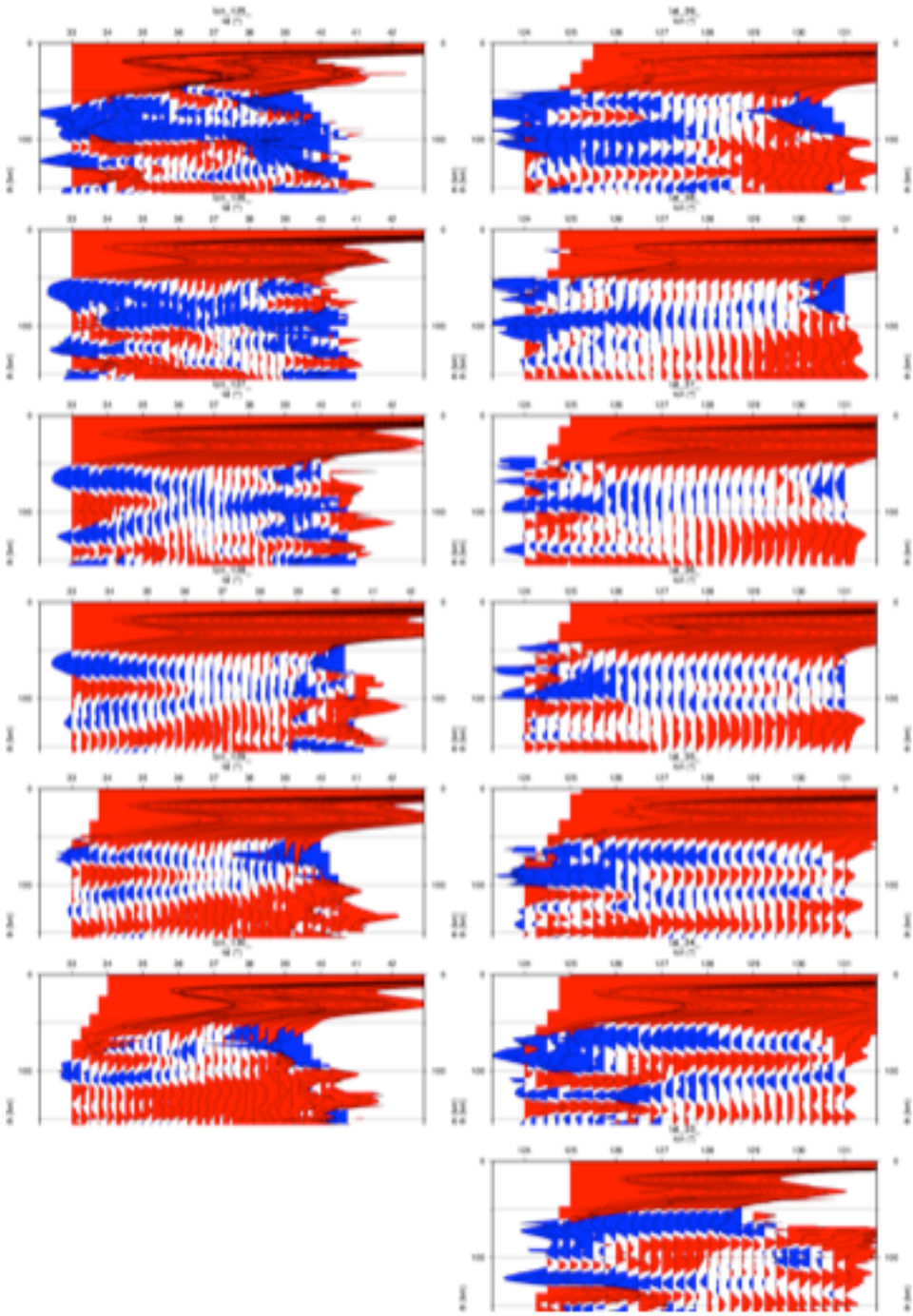

FIGURE 13. SECTIONS OF THE COMMON CONVERSION POINT (CCP) STACKED S RECEIVER FUNCTIONS (SRFS) ALONG THE LONGITUDES AND THE LATITUDES. THE POSITIVE AND THE NEGATIVE SIGNALS ARE COLORED IN RED AND BLUE, RESPECTIVELY.

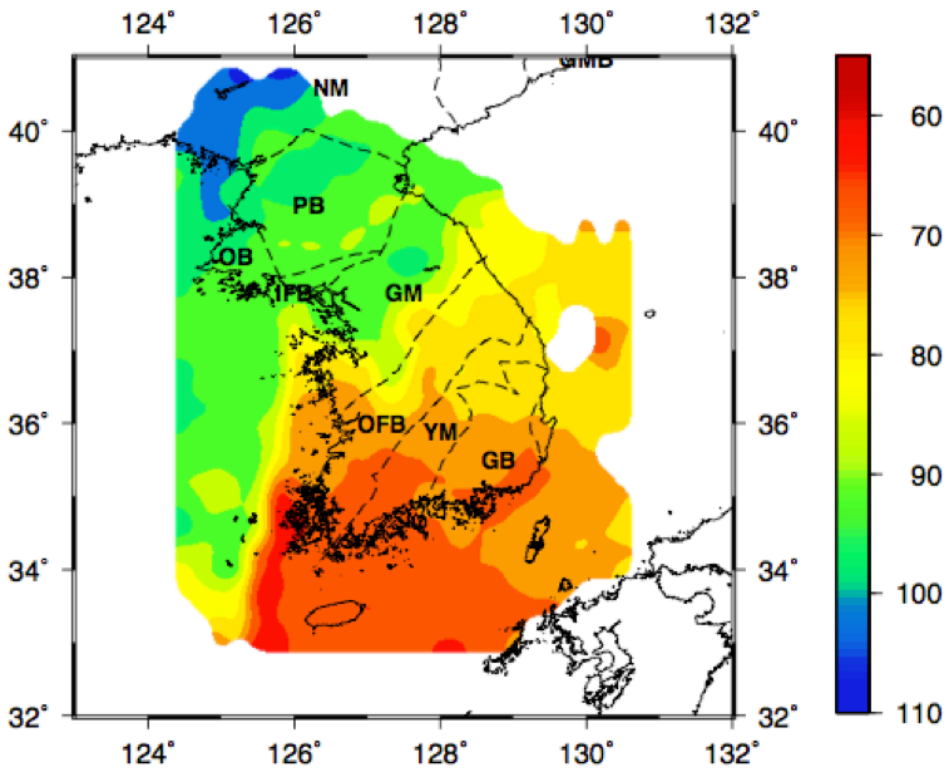

FIGURE 14. TOPOGRAPHY OF THE LITHOSPHERE-ASTHENOSPHERE BOUNDARY (LAB).

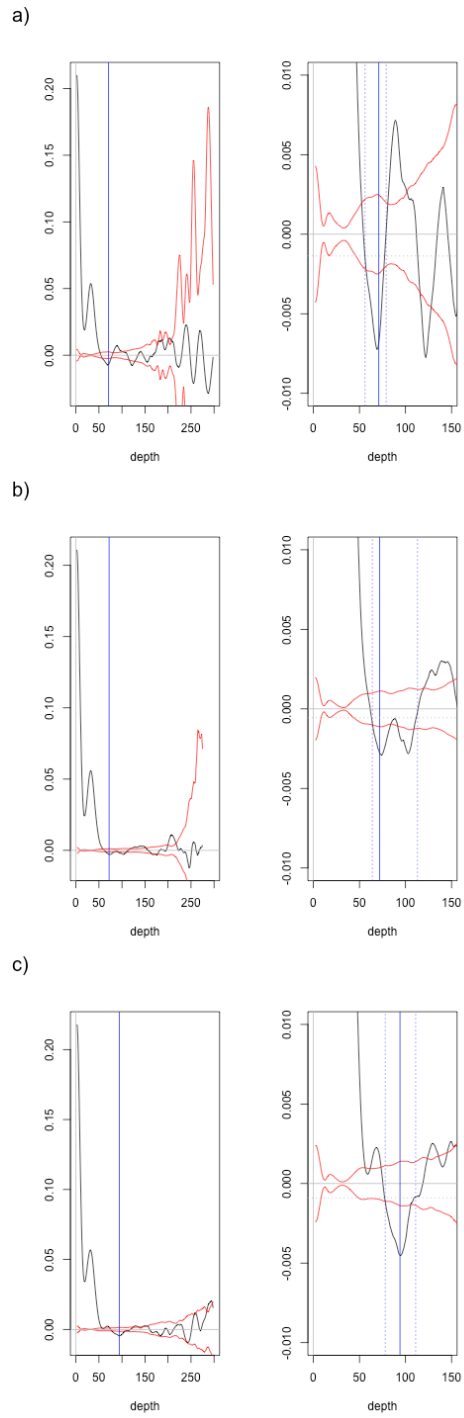

FIGURE 15. EXAMPLES OF THE LITHOSPHERE-ASTHENOSPHERE BOUNDARY (LAB) DEPTH ESTIMATION UNCERTAINTY. THE COMMON CONVERSION POINT (CCP) STACKED RECEIVER FUNCTIONS(SRFS) AT (A) (34° N, 127° E), (B) (36° N, 127° E) AND (C) (38° N, 127° E) ARE SHOWN IN BLACK WITH THE STANDARD ERROR IN RED. THE SOLID BLUE VERTICAL LINE REPRESENTS THE DEPTH OF THE PICKED LAB, WHILE THE DASHED BLUE LINE REPRESENTS THE BOUNDS OF

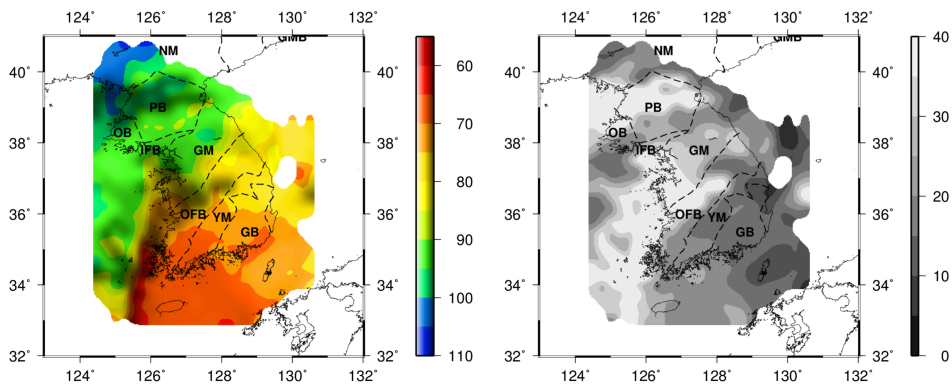

FIGURE 16. (A) LITHOSPHERE-ASTHENOSPHERE BOUNDARY (LAB) DEPTH ILLUMINATED BY THE (B) UNCERTAINTY.

DISCUSSION

The double negative phases are observed in the southern part of the Korean Peninsula. A single negative discontinuity at different depths in the vicinity could be shown as double negative phases when the stacking bin size is large. The robust signals with comparable amplitudes with the negative phase in the northern part (N1) indicate that the double negative phases represent real structure. For further verification, non-overlapping bins with 1° by 1° in the latitude and the longitude are used in CCP stacking (Figure 17). Because of the small size of the bins, the CCP stacked receiver functions are more unstable, and the robust amplitude determined by the bootstrap test is weaker. In spite of the instability, the features of the LAB in the Korean Peninsula are reproduced well.

The time-domain deconvolution method is free from a side-lobe because of the use of a Gaussian function. Nevertheless, the forward modeling of the SRF is performed to assess possible artifacts. First, synthetic teleseismic seismograms are generated with the YASEIS program [*Ma*, 2013]. The synthetic seismograms are used then to calculate synthetic SRFs. A simplified 1-D velocity model is used for modeling the teleseismic seismograms. The 1-D model is generated by modifying the IASP91 model. The P- and the S-wave velocities are proportionally modified so that the Vp/Vs ratio remains constant. The synthetics are calculated at epicentral distances from 59° to 86° with 1° spacing. Figure 19 shows the synthetic seismograms for events at

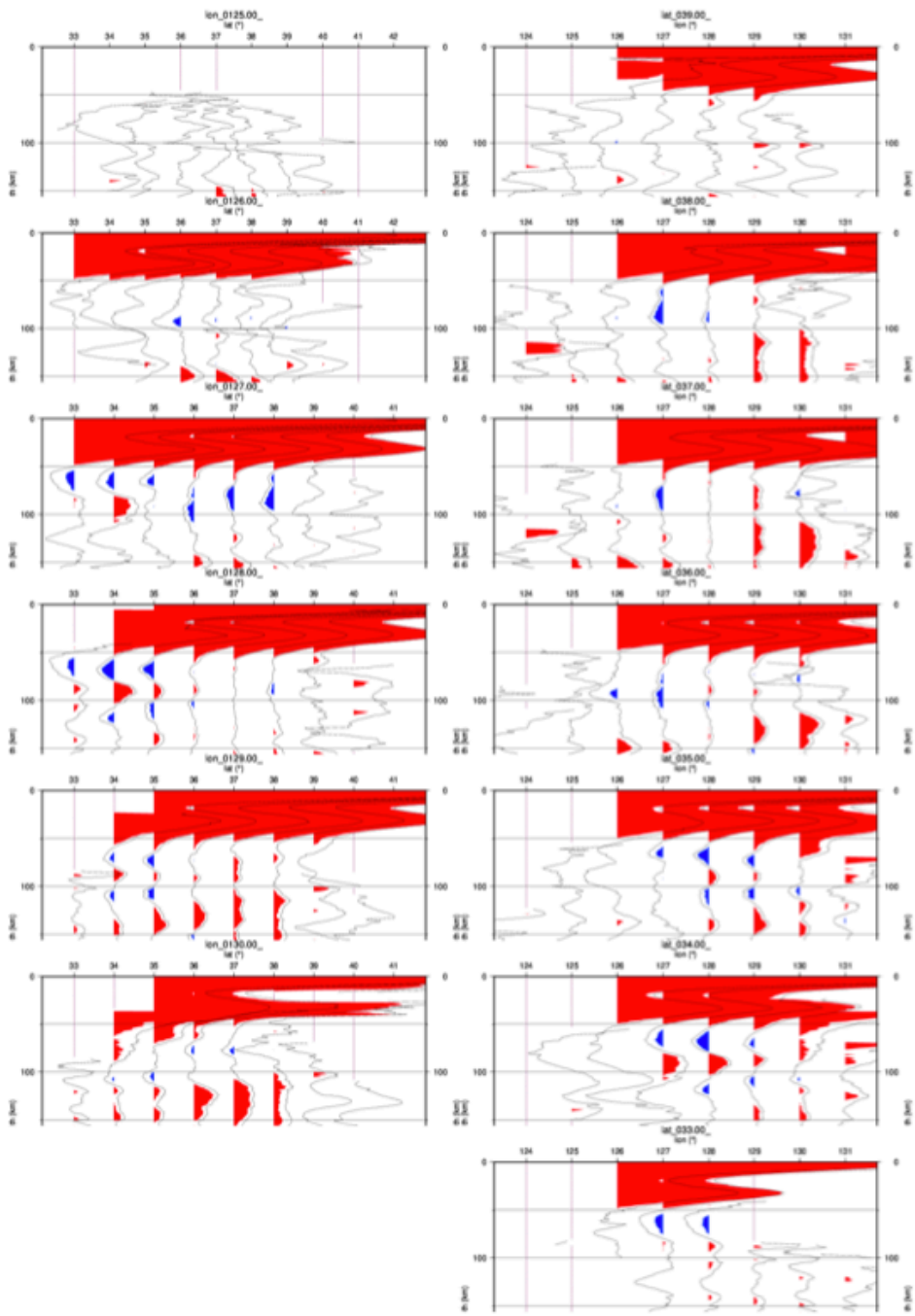

FIGURE 17. SECTIONS OF COMMON CONVERSION POINT (CCP) STACKING S RECEIVER FUNCTION (SRFS) ALONG THE LONGITUDES AND THE LATITUDES. LATERALLY, THE GRID OF THE STACKING POINTS IS 1° BY 1°, AND A SQUARE BIN WITH SIZE OF 1° BY 1° IS USED WITHOUT OVERLAP.

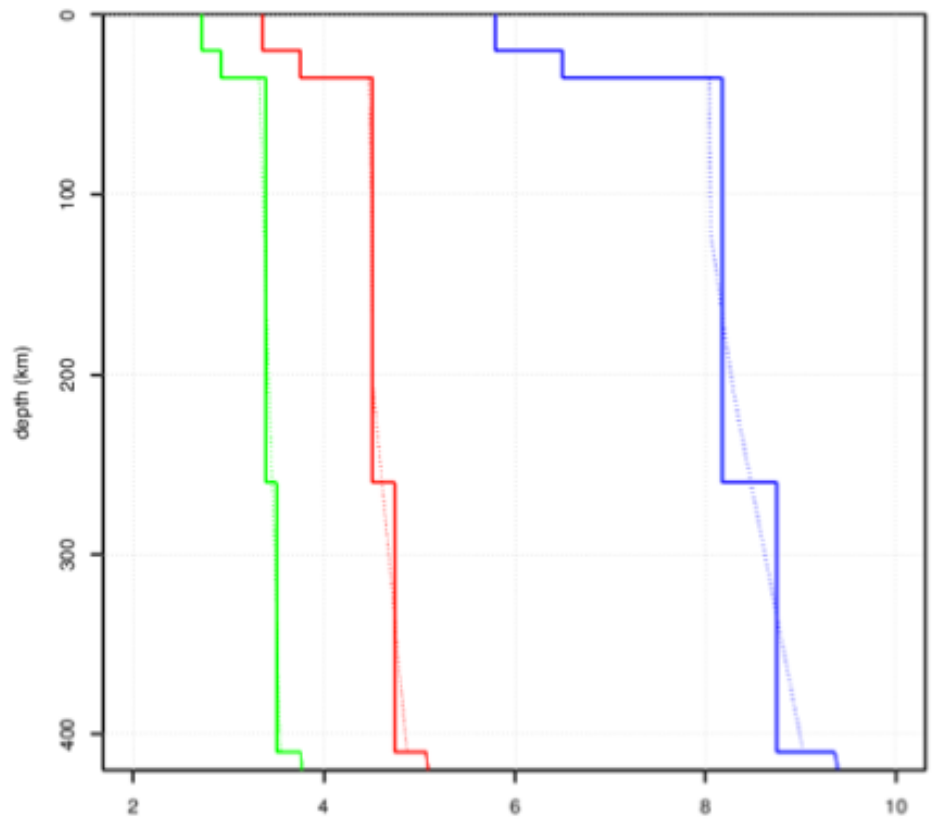

FIGURE 18. SIMPLIFIED 1-D MODEL USED IN FORWARD MODELING OF THE SYNTHETIC TELESEISMIC SEISMOGRAMS. THE BLUE, RED, AND GREEN LINES REPRESENT VP (KM/S), VS (KM/S), AND DENSITY (G/CM^3), RESPECTIVELY. THE DOTTED LINE SHOWS THE VALUES OF THE IASP91 MODEL.

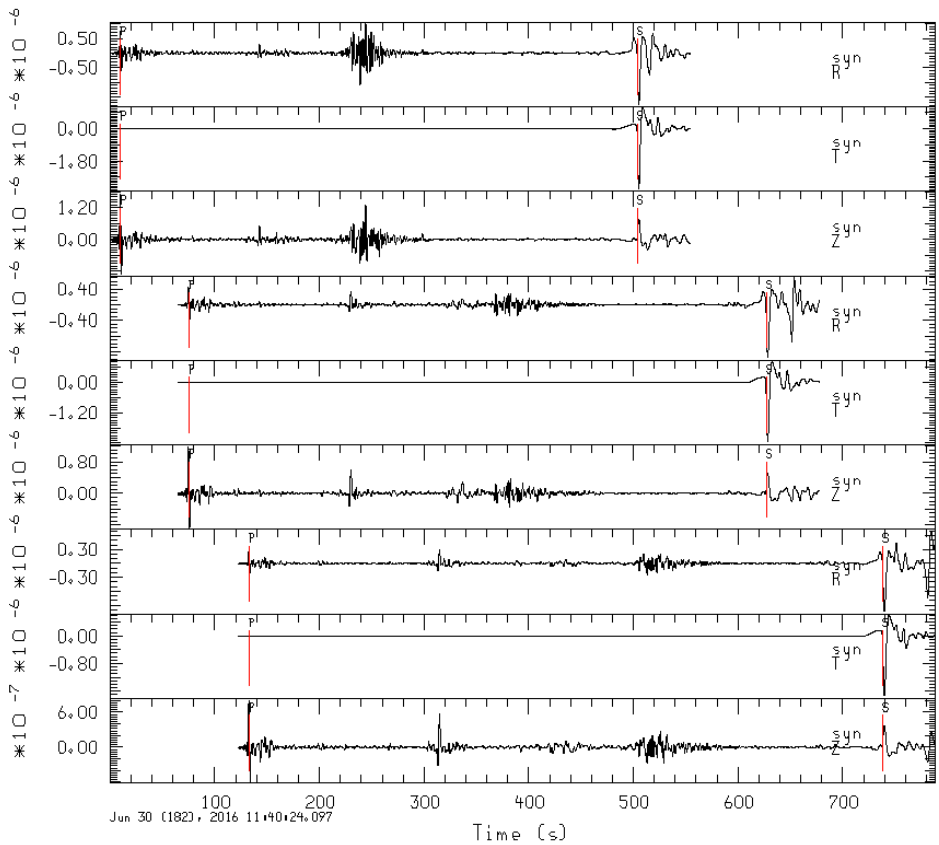

FIGURE 19. EXAMPLES OF THE SYNTHETIC TELESEISMIC SEISMOGRAMS FOR THE EVENTS WITH EPICENTRAL DISTANCES OF 60°, 70°, AND 80° WITH THE IASP91 MODEL. EACH SET OF SEISMOGRAMS IS IN THE ORDER OF RADIAL, TRANSVERSE AND VERTICAL COMPONENTS.

epicentral distances of 60°, 70°, and 80°. From the synthetic seismograms, the SRFs are calculated like the observed seismograms (Figure 20). In the section of the synthetic SRFs (Figure 20), the phases converted at the Moho, the 260-km discontinuity, and the 410-km discontinuity are observed. Additional phases are recognized, too. By migrating the SRFs and applying the CCP stacking method, the signals, except those converted at the Moho and the 260-km discontinuity, are effectively suppressed as shown in Figure 21. The synthetic tests for structures with single and double low velocity layers (Figure 22 and Figure 24) are presented in Figure 23 and Figure 25. The observations in the northern part are explained by a single low velocity layer, while those in the southern part are explained by double low velocity layers.

Figure 26 and Figure 27 show the representative CCP stacked receiver functions at (34° N, 127° E) and (38° N, 127° E) with corresponding synthetic receiver functions for the southern part and the northern part, respectively. The velocity reduction of 2-3 % for the low velocity layer produces almost comparable amplitudes. The double negative signals in the southern part can be produced by double low velocity layers. This means that the double negative phases shown in the CCP stacked receiver functions are not an artifact of the side-lobes. At the depth range of the 120 - 200 km, a broad negative signal appears for the IASP91 model, even though there is no negative velocity layer. This artificial negative signal is produced because unwanted phases, such as ScS410p and SKS 410p, are not completely eliminated by the stacking. In the result, the negative signals appear at

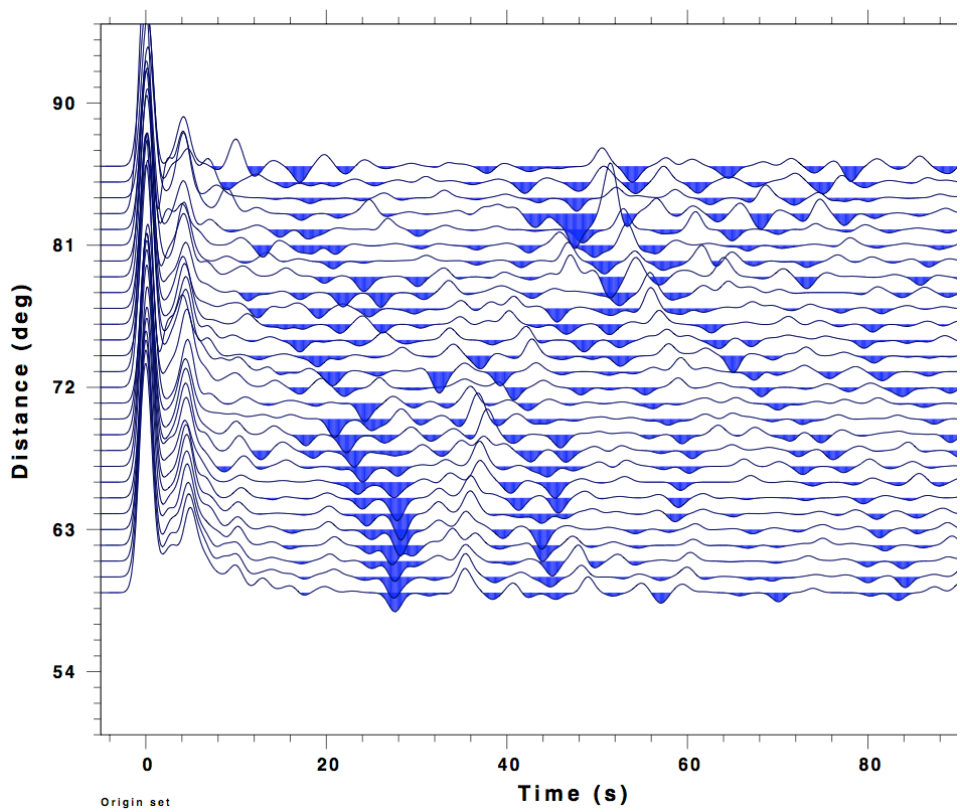

FIGURE 20. SECTION OF SYNTHETIC S RECEIVER FUNCTIONS (SRFS) CALCULATED WITH THE MODEL IN FIGURE 18.

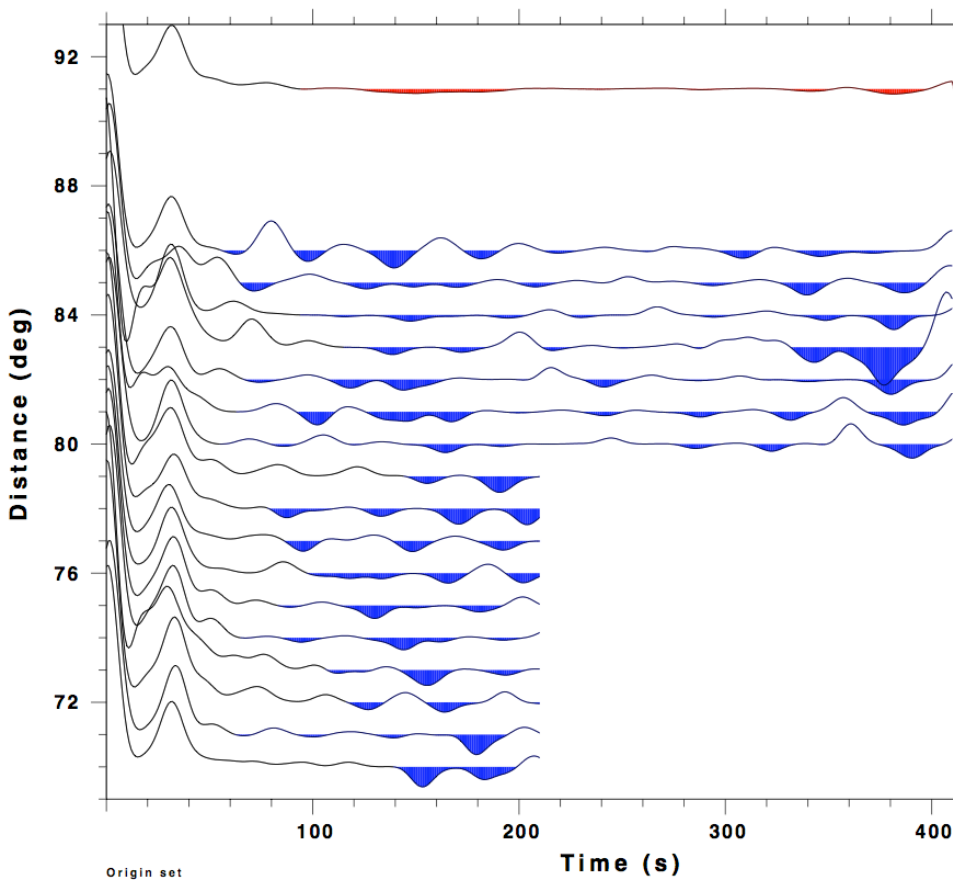

FIGURE 21. MIGRATED SYNTHETIC S RECEIVER FUNCTIONS (SRFS) AND THE STACKED ONE. THE DELAYED TIMES OF THE SYNTHETIC S RECEIVER FUNCTIONS (SRFS) IN FIGURE 20 ARE MIGRATED TO CORRESPONDING CONVERSION POINTS ACCORDING TO THE SIMPLIFIED MODEL IN FIGURE 18.

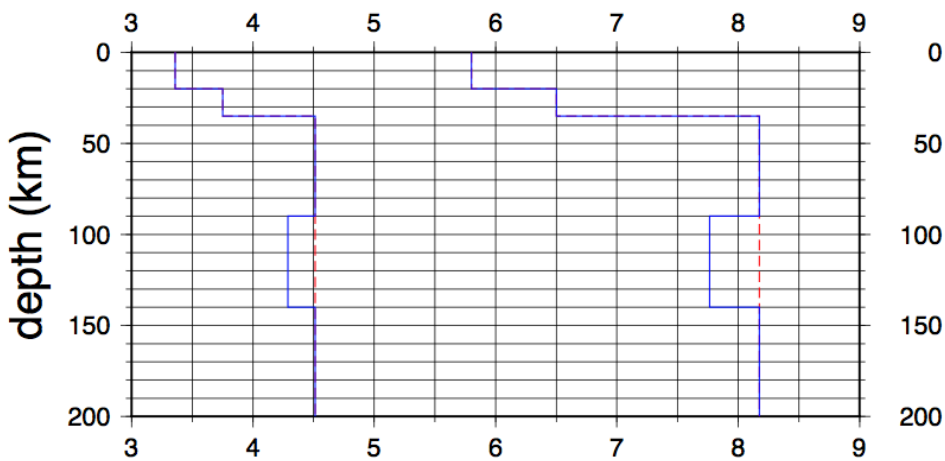

FIGURE 22. SIMPLE VP AND VS MODEL WITH A SINGLE LOW VELOCITY LAYER.

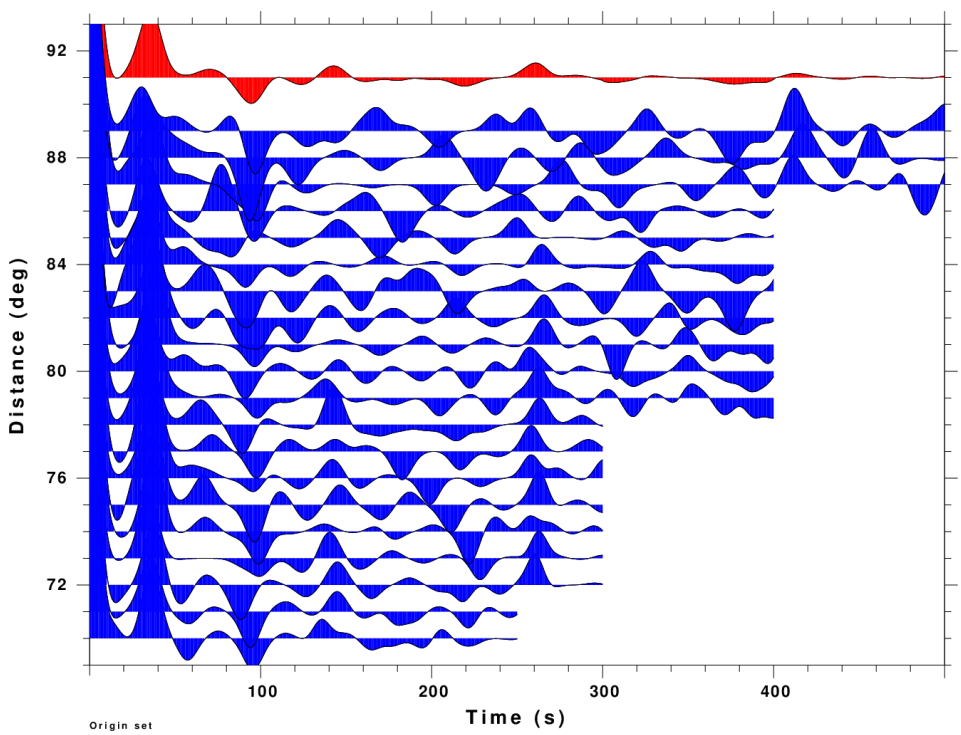

FIGURE 23. MIGRATED SYNTHETIC S RECEIVER FUNCTIONS (SRFS) AND THE STACKED ONE. THE SYNTHETIC S RECEIVER FUNCTIONS (SRFS) CALCULATED WITH THE MODEL IN FIGURE 22 ARE MIGRATED TO CORRESPONDING CONVERSION POINTS ACCORDING TO THE SIMPLIFIED MODEL IN FIGURE 18.

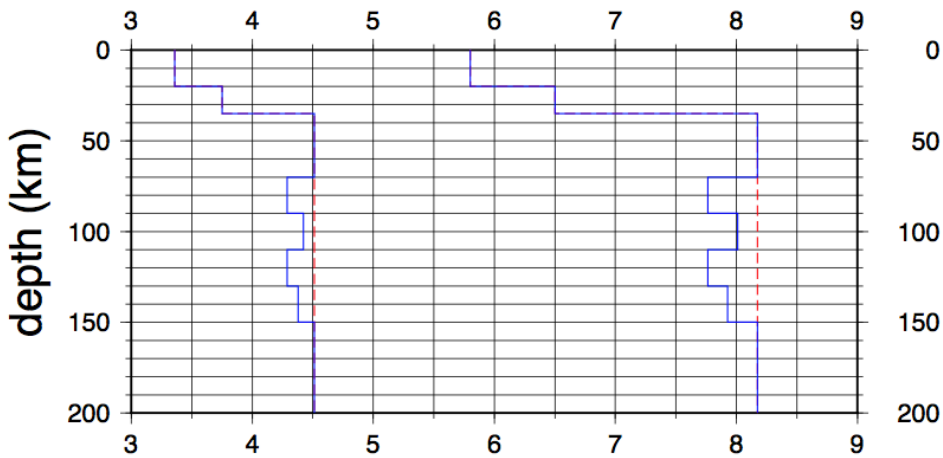

FIGURE 24. SIMPLE VP AND VS MODEL WITH TWO LOW VELOCITY LAYERS.

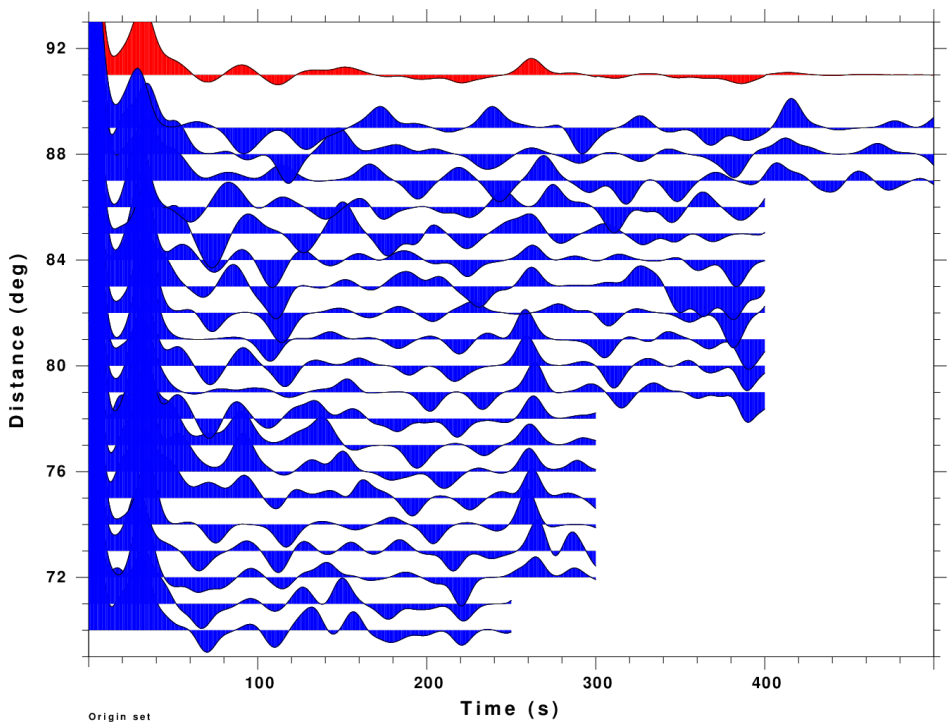

FIGURE 25. MIGRATED SYNTHETIC S RECEIVER FUNCTIONS (SRFS) AND THE STACKED ONE. THE SYNTHETIC S RECEIVER FUNCTIONS (SRFS) CALCULATED WITH THE MODEL IN FIGURE 24 ARE MIGRATED TO CORRESPONDING CONVERSION POINTS ACCORDING TO THE SIMPLIFIED MODEL IN FIGURE 18.

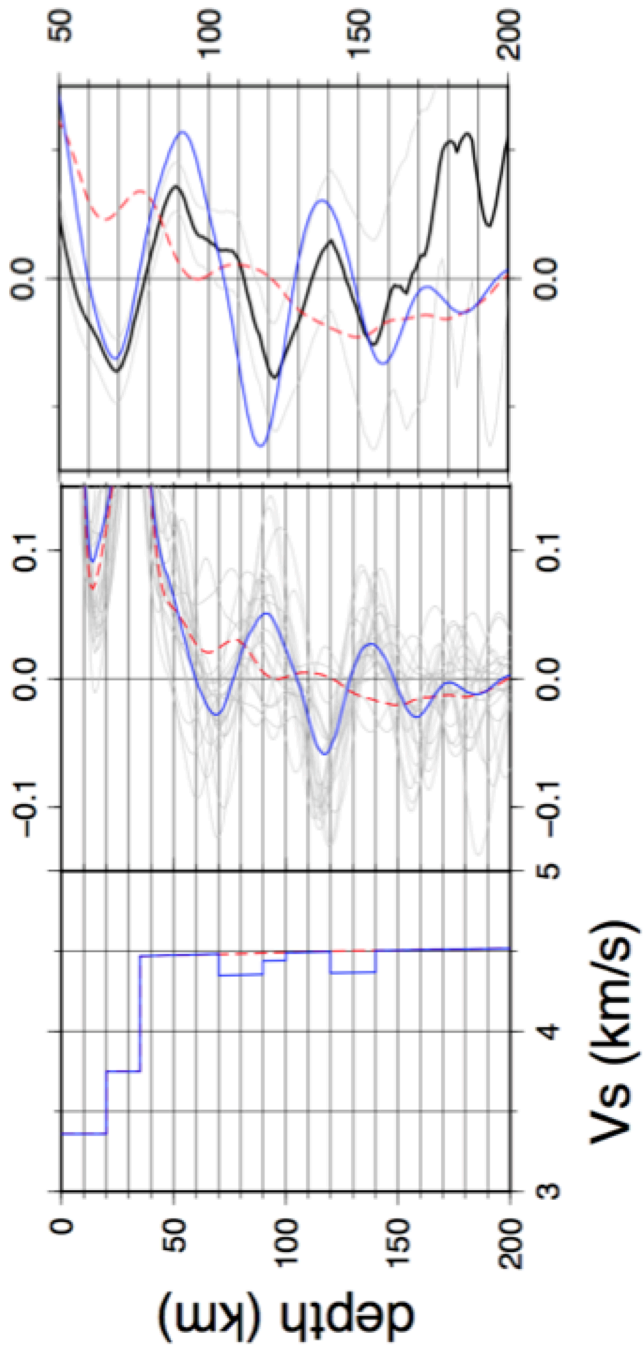

FIGURE 26. COMMON CONVERSION POINT (CCP) STACKED RECEIVER FUNCTION OBTAINED AT (34° N, 127° E) WITH STACKED RECEIVER FUNCTIONS OBTAINED FROM THE SYNTHETIC TELESEISMIC SEISMOGRAMS. THE RED AND BLUE LINES REPRESENT THE RECEIVER FUNCTIONS FOR THE IASP91 AND THE PREFERRED MODEL, RESPECTIVELY. THE GRAY WAVELETS IN THE MIDDLE PLOT SHOW ALL RECEIVER FUNCTIONS STACKED FOR THE PREFERRED MODEL. THE CORRESPONDING S-WAVE VELOCITY MODEL IS SHOWN AT THE BOTTOM.

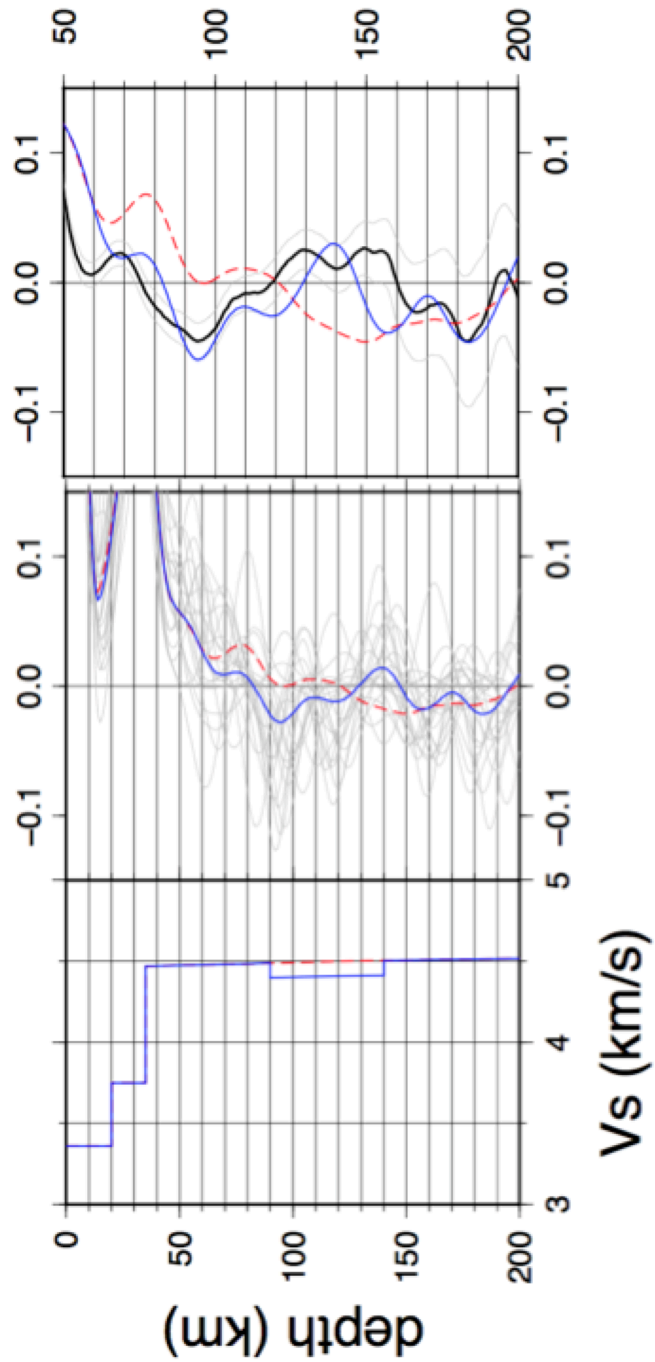

FIGURE 27. COMMON CONVERSION POINT (CCP) STACKED RECEIVER FUNCTION OBTAINED AT (38° N, 127° E) WITH STACKED RECEIVER FUNCTIONS OBTAINED FROM THE SYNTHETIC TELESEISMIC SEISMOGRAMS. THE RED AND BLUE LINES REPRESENT THE RECEIVER FUNCTIONS FOR THE IASP91 AND THE PREFERRED MODEL, RESPECTIVELY. THE GRAY WAVELETS IN THE MIDDLE PLOT SHOW ALL RECEIVER FUNCTIONS STACKED FOR THE PREFERRED MODEL. THE CORRESPONDING S-WAVE VELOCITY MODEL IS SHOWN AT THE BOTTOM.

different depths with narrow widths. This implies that the negative signals shown in the CCP stacked receiver functions represent real discontinuities beneath the study area.

The LAB beneath the Korean Peninsula is imaged applying the CCP stacking method to the SRFs. Below the Moho at 35 km depth, negative signals correspond to the negative discontinuity where the velocity drops downwards in the uppermost mantle (Figure 11 and Figure 12). The negative phases named as S1 and N1 are dominant with lateral continuity over the entire study area. These dominant negative phases are interpreted as the LAB beneath the Korean Peninsula. The depth of the LAB ranges from 60 km to 100 km. The distribution of the LAB depth shows two modes at ~70 km depth and ~92 km depth (Figure 28). This shallow depth is consistent with the LAB depth determined to be shallower than 70 km depth from previous global studies [*Artemieva and Mooney*, 2001; *An and Shi*, 2006; *Artemieva*, 2006; *Pandey et al.*, 2014]. This is also consistent with the LAB determined to be at 70 km depth in China adjacent to the study area [*Sodoudi et al.*, 2006; *Kind et al.*, 2012].

The LAB depth in the Korean Peninsula is much shallower than that expected for Precambrian cratons [*Artemieva and Mooney*, 2001]. A depth of the LAB shallower than 110 km implies an occurrence of lithosphere thinning. The mechanism of the lithosphere thinning is mainly explained by two models: one is the lithosphere delamination and the other is the lithosphere

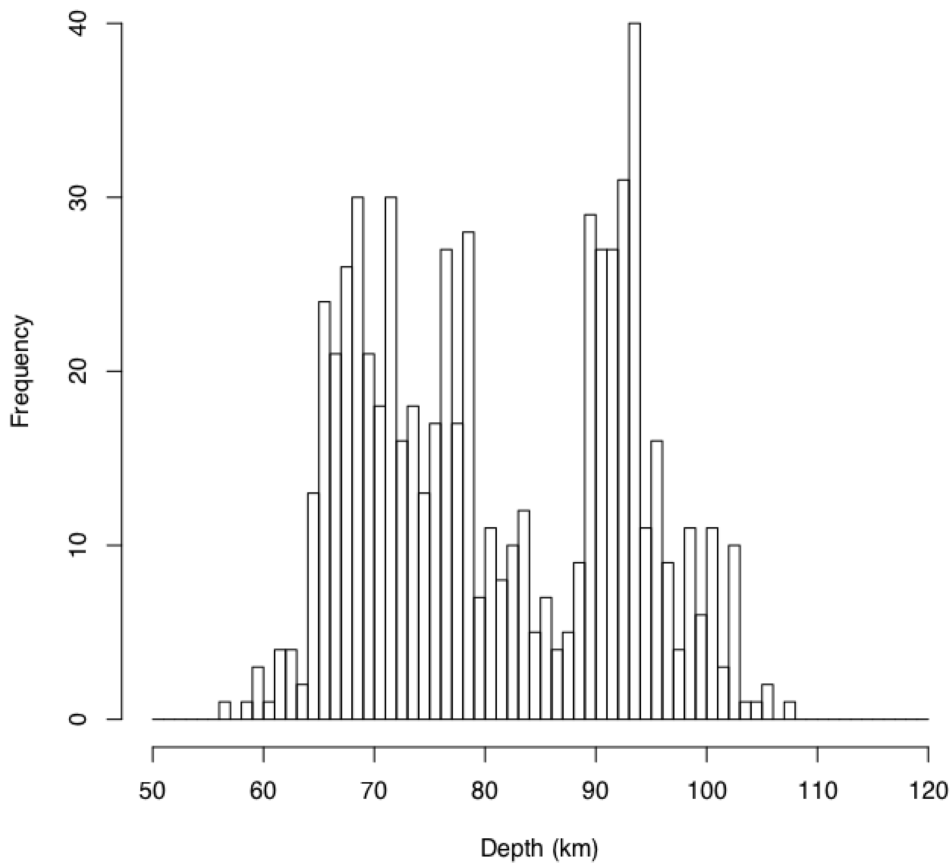

FIGURE 28. DISTRIBUTION OF THE LITHOSPHERE-ASTHENOSPHERE BOUNDARY(LAB) DEPTH IN AND AROUND THE KOREAN PENINSULA.

erosion. The thin lithosphere (< 100 km) in eastern China is regarded as a result of lithosphere thinning [*Xu et al.*, 2000; *Wu et al.*, 2005; *Xu*, 2007; *Zhu et al.*, 2012; *Tang et al.*, 2013]. From the intensive development of the Early Cretaceous magmatism, the lithosphere is destroyed during that time period with close relation to the mantle convection induced by the subducting Pacific slab beneath the Asian Plate [*Zhu et al.*, 2012]. In the Korean peninsula, the Phanerozoic granitoids are widely distributed [*Cheong and Kim*, 2012]. Intensive magmatism is developed during the Jurassic. This massive Jurassic magmatism is regarded as a indication of the lithosphere thinning in the Korean Peninsula [*Kee et al.*, 2010]. According to the reconstruction model [*Seton et al.*, 2015], the oceanic Izanagi Plate was subducting northwestward beneath the Asian Plate. The upwelling of the mantle induced by the subducting slab eroded the lower lithosphere.

Along the profile line AA' (Figure 11), a nearly flat LAB is observed at ~75 km depth in the southern part (S1) and at ~95 km depth in the northern part (N1). Another negative phase is observed at the depth of 110 km in the southern part (S2). The transition zone of LAB dipping northwards from the S1 to the N1 is observed between the N1 and S1. The location of the transition zone is roughly overlapping with the OFB. Along another profile line shifted by 1° westward from the profile line AA', an identical feature of the LAB also appears but the location is migrated to the south (Figure 29). This migration of the transition zone is consistent with the NE-SW extent of the tectonic boundaries at the surface. This implies that the LAB is shallower at the south

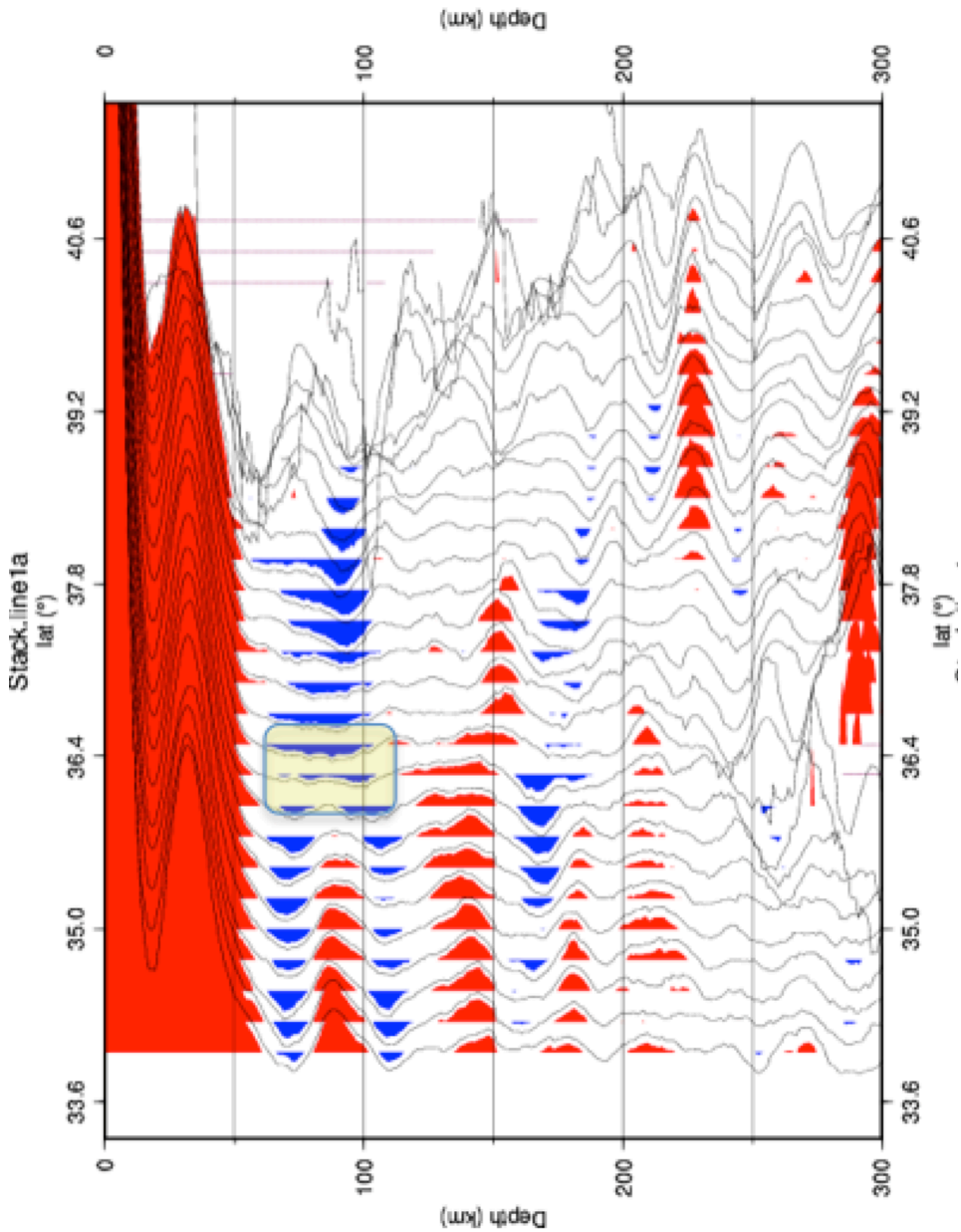

FIGURE 29. COMMON CONVERSION POINT (CCP) STACKED S RECEIVER FUNCTIONS (SRFS) ALONG THE LINE SHIFTED 1° WESTWARD PARALLEL TO THE PROFILE AA'.

and deeper at the north with a transition zone beneath the OFB. The rapid change of the LAB depth shown in the transition zone is revealed in the topography map in Figure 14 along the tectonic boundary between the OFB and GM.

Previously, the shallow depth of the LAB beneath the Korean Peninsula was explained by the lithosphere thinning implied by the massive Jurassic magmatism [*Cheong and Kim*, 2012]. However, this lithosphere thinning cannot explain the distinct difference of the LAB depth in the northern block and the southern block. Since the Jurassic magmatism is distributed at both blocks, it is not likely that only the lithosphere of the southern part is destroyed. The shallow depth of the LAB at the northern block requires lithosphere thinning. Furthermore, the Mesozoic magmatism shows no distinguishable difference across the OFB implying a significant difference in lithosphere thinning. In the absence of significant difference in magmatism, the difference in the lithosphere thickness could be originated from the different nature of the lithosphere across the transition zone. This suggests that the northern block and the southern block have distinctive tectonic history.

Although the boundary is still debated, the Korean Peninsula is regarded as an amalgam of the SKB and the SCB via the continental collision that occurred from the Permian and the Triassic. Several models are proposed for the continental collision geologically [*Chough et al.*, 2013; *Oh et al.*, 2015] and

seismologically [*Chang and Baag*, 2007; *Yoo et al.*, 2007; *Hong and Choi*, 2012]. The transition zone of the LAB separating the northern part and the southern part might indicate a collision boundary between the SKB and the SCB. In addition, the distinct feature shown in the LAB topography might indicate that the lithospheric structure was different between the SKB and the SCB. The transition zone might indicate the collisional boundary between the SKB and the SCB. The double negative phases in the southern part might indicate that the lithosphere of the southern part is overriding the lithosphere of the northern block subducted during the collision as observed beneath the Tibetan Platform [*Zhao et al.*, 2011]. However, this interpretation contradicts the following lithosphere thinning, not only in the Korean Peninsula during the Jurassic, but also in eastern China during the Cretaceous. It is hardly reasonable that the structure formed during the continental collision would remain after the following lithosphere delamination or erosion of lower lithosphere.

Kim et al. [2015] proposed a model of corner flow by the subduction of the Izanagi Plate from the mantle plume at the northwest. The supply of the hot mantle could contribute to the lithosphere thinning at the Korean Peninsula. But the source of the hot mantle at the north does not properly explain the shallower LAB in the southern part.

Around 60 Ma in the Early Cenozoic, the oceanic ridge between the Izanagi Plate and the Pacific Plate is subducted beneath the Eurasian Plate [*Whittaker*

et al., 2007; *Seton et al.*, 2015]. While the ridge subducts, a slab window could be opened where hot mantle can flow in [*Thorkelson and Taylor*, 1989]. The inflow of the hot mantle from the south can explain the shallow LAB at the southern part. The double negative phases in the southern part may indicate that the lithosphere is depleted with the asthenosphere upwelling. The depleted lithosphere might be imaged as a sequence of the positive and the negative signals beneath the LAB in the southern part. However, the absence of a corresponding difference in the magmatism still remains unsolved.

During the Miocene, the Korea Strait is formed by a back-arc rift system. The extensional force stretches the lithosphere and induces upwelling of the asthenosphere. The slow velocity anomaly for the asthenosphere along the Korea Strait is reported by *Kim et al.* [2016, submitted]. The LAB depth decreases at the Korea Strait, especially around Jeju Island. This indicates that the back-arc rift system affected the lithosphere in the Korea Strait. However, this event is not enough to explain the inland deformation of the lithosphere structure.

Shin et al. [2012] proposed a sinusoidal undulation of folded lithosphere induced by compressional force developed by the collision and subduction. However, a corresponding sinusoidal variation is not observed in the LAB topography.

CONCLUSION

The LAB structure beneath the Korean Peninsula is imaged from the teleseismic SRF using the CCP stacking method. A shallow LAB is revealed with a depth ranging from 60 km to 105 km. The depth of the LAB shows a large difference between the northern part and the southern part with the boundary consistent with the surficial tectonic boundary between the GM and the OFB. Furthermore, beside the single negative phase around a 70 km depth in the northern part, two distinct negative phases are imaged in the southern part. From the resolved LAB structure of the Korean Peninsula, the lithosphere structure is recognized to be altered by the subduction of the oceanic plates (the Izanagi Plate and the Pacific Plate).

The shallow depth (<100 km) of the LAB in the Korean Peninsula is much thinner than that expected for the Precambrian craton. This thin lithosphere supports that the lithosphere thinning was facilitated by the coeval subduction of the Izanagi Plate in the Jurassic. The distinct structure of the LAB between the northern part and the southern part cannot be explained by existing tectonic models of the Korean Peninsula. The LAB structure resembles what is developed through continental collision as in Tibet. However, chronologically, the remnant of the collision in the Permian cannot remain after the lithosphere thinning that accompanied massive magmatism in the Jurassic. The subduction of the oceanic ridge at ~60 Ma could be a candidate for the additional delamination of the southern lithosphere.

However, the corresponding change in the magmatism is not observed. Other tectonic models do not explain the development of the LAB structure beneath the Korean Peninsula either. More comprehensive and multidisciplinary information is required to understand the lithosphere structure in the Korean Peninsula. The resolved structure of the lithosphere and the asthenosphere of the Korean Peninsula can be used to understand the tectonic history of the Korean Peninsula.

SUMMARY

In this thesis, the receiver function technique is used to study the seismic discontinuities beneath the Korean Peninsula. A common conversion point stacking method is applied to image the discontinuities in the upper mantle, i.e., at 410 km and 660 km, and the lithosphere-asthenosphere boundaries. The origins of the resolved structure of the upper mantle beneath the Korean Peninsula are discussed with the tectonic history and the tectonic environment of the Korean Peninsula.

In Part I, topography of the 410 km and the 660 km discontinuities were determined using the teleseismic P-receiver functions. Positive correlations between the topography of the discontinuities and the cold Pacific slab are identified. Additionally, complex features are observed in both discontinuities. Where the slab penetrates 410 km, the 410 km discontinuity is elevated by the low temperature of the slab. There is a gap, and the gap is well matched with the location of the slab tear. A highly depressed 410 km discontinuity observed behind the slab supports an upwelling of the mantle at the location. The depressed discontinuity over a broad area beyond the slab could be a remnant of the retreat of the Japan Trench. The 660 km discontinuity appears to be depressed by the low temperature of the stagnant slab above it. Although the extension is limited in small areas, a large depression of ≥ 40 km is observed in some locations. The large depression implies that a small portion of the slab penetrates the 660 km discontinuity and sinks into the

lower mantle while most of the slab is trapped in the mantle transition zone above the discontinuity. The most impressive feature shown in the topography is that north of 38° N it is not depressed though the cold slab exists at all latitudes. This difference could be originated by the difference in the subducting angle between the Japan Trench and the Izu-Bonin Trench. In addition, the difference could be explained by the difference in the water content. The weak depression of the 660 km discontinuity to the north of 38° N might be an indication that the water content is lower than in the south.

In Part II, the structure of the LAB is imaged using the teleseismic S-receiver functions. Negative phases, representing a discontinuity of velocity reduction with depth, are observed at a depth range of 60 - 120 km. The depth of the LAB beneath the Korean Peninsula is determined to be thin for the Precambrian bedrock. The thin lithosphere implies a lithosphere thinning in the Mesozoic when the paleo-Pacific subducts beneath the Korean Peninsula accompanying massive magmatism. A distinct difference in the structure of the LAB is observed at the north and the south across the tectonic boundary of the GM and the OFB. The depth of the LAB is deeper at the north and shallower at the south. The depth changes rapidly along the tectonic boundary between the GM and the OFB. At the south, an additional negative discontinuity is observed beneath the LAB. This implies the existence of two low velocity layers at the south. The vertical section of the CCP stacked receiver function resembles what is formed by continental collision. However, the continental collision between the Sino-Korean Block and the South China

Block had finished in the early Triassic, and the lithosphere thinning occurred in the Jurassic that followed. Therefore, the continental collision could not be a cause of the LAB structure beneath the Korean Peninsula. The subduction of the oceanic ridge between the Izanagi Plate and the Pacific Plate could explain the LAB structure at the south. The upwelling through the gap of the slab, opened by the subduction of the oceanic ridge, might have triggered the lithosphere delamination in the south of the Korean Peninsula. However, the absence of corresponding evidence for the magmatism cannot be explained. Any existing tectonic model of the Korean Peninsula cannot explain the LAB structure and the magmatism simultaneously. The resolved LAB structure beneath the Korean Peninsula could contribute to understanding and establishing the tectonic history of the Korean Peninsula.

REFERENCES

Abdelwahed, M. F., and D. Zhao (2007), Deep structure of the Japan subduction zone, *Phys. Earth Planet. Inter.*, *162*(1–2), 32–52, doi:10.1016/j.pepi.2007.03.001.

Ai, Y., and T. Zheng (2003), The upper mantle discontinuity structure beneath eastern China, *Geophys. Res. Lett.*, *30*(21), 2089, doi:10.1029/2003GL017678.

Ai, Y., T. Zheng, W. Xu, Y. He, and D. Dong (2003), A complex 660 km discontinuity beneath northeast China, *Earth Planet. Sci. Lett.*, *212*(1–2), 63–71, doi:10.1016/S0012-821X(03)00266-8.

An, M., and Y. Shi (2006), Lithospheric thickness of the Chinese continent, *Phys. Earth Planet. Inter.*, *159*(3-4), 257–266, doi:10.1016/j.pepi.2006.08.002.

Artemieva, I. M. (2006), Global 1° × 1° thermal model TC1 for the continental lithosphere: Implications for lithosphere secular evolution, *Tectonophysics*, *416*(1–4), 245–277, doi:10.1016/j.tecto.2005.11.022.

Artemieva, I. M., and W. D. Mooney (2001), Thermal thickness and evolution of Precambrian lithosphere: A global study, *J. Geophys. Res. Solid Earth*, *106*(B8), 16387–16414, doi:10.1029/2000JB900439.

Bagley, B., A. M. Courtier, and J. Revenaugh (2009), Melting in the deep upper mantle oceanward of the Honshu slab, *Phys. Earth Planet. Inter.*, *175*(3–4), 137–144, doi:10.1016/j.pepi.2009.03.007.

Bassin, C., G. Laske, and G. Masters (2000), The current limits of resolution for surface wave tomography in North America, *Eos Trans. Am. Geophys. Union*, *81*, F897.

Bijwaard, H., W. Spakman, and E. R. Engdahl (1998), Closing the gap between regional and global travel time tomography, *J. Geophys. Res. Solid Earth*, *103*(B12), 30055–30078, doi:10.1029/98JB02467.

Brudzinski, M., W. Chen, R. Nowack, and B. Huang (1997), Variations of P wave speeds in the mantle transition zone beneath the northern Philippine Sea, *J. Geophys. Res.-Solid Earth*, *102*(B6), 11815–11827, doi:10.1029/97JB00212.

Cao, A., and A. Levander (2010), High-resolution transition zone structures of the Gorda Slab beneath the western United States: Implication for deep water subduction, *J. Geophys. Res. Solid Earth*, *115*(B7), B07301, doi:10.1029/2009JB006876.

Chang, S.-J., and C.-E. Baag (2007), Moho Depth and Crustal VP/VS Variation in Southern Korea from Teleseismic Receiver Functions: Implication for Tectonic Affinity between the Korean Peninsula and China, *Bull. Seismol. Soc. Am.*, *97*(5), 1621–1631, doi:10.1785/0120050264.

Cheong, C.-S., and N.-H. Kim (2012), Review of Radiometric Ages for Phanerozoic Granitoids in Southern Korean Peninsula, *J. Petrol. Soc. Korea*, *21*(2),

doi:10.7854/JPSK.2012.21.2.173.

Chough, S. K., D. J. Lee, and J.-H. Ree (2013), Whereabouts of the collision belt between the Sino-Korean and South China blocks in the northeast Asian margin, *Geosci. J.*, *17*(4), 397–401, doi:10.1007/s12303-013-0057-4.

DeMets, C., R. G. Gordon, D. F. Argus, and S. Stein (1994), Effect of recent revisions to the geomagnetic reversal time scale on estimates of current plate motions, *Geophys. Res. Lett.*, *21*(20), 2191–2194, doi:10.1029/94GL02118.

Fukao, Y., M. Obayashi, H. Inoue, and M. Nenbai (1992), Subducting slabs stagnant in the mantle transition zone, *J. Geophys. Res. Solid Earth*, *97*(B4), 4809–4822, doi:10.1029/91JB02749.

Fukao, Y., S. Widiyantoro, and M. Obayashi (2001), Stagnant slabs in the upper and lower mantle transition region, *Rev. Geophys.*, *39*(3), 291–323, doi:10.1029/1999RG000068.

Fukao, Y., M. Obayashi, and T. Nakakuki (2009), Stagnant slab: A review, *Annu. Rev. Earth Planet. Sci.*, *37*(1), 19–46, doi:10.1146/annurev.earth.36.031207.124224.

Gudmundsson, O., and M. Sambridge (1998), A regionalized upper mantle (RUM) seismic model, *J. Geophys. Res. Solid Earth*, *103*, 7121–7136, doi:10.1029/97jb02488.

Higo, Y., T. Inoue, T. Irifune, and H. Yurimoto (2001), Effect of water on the spinel-postspinel transformation in Mg2SiO4, *Geophys. Res. Lett.*, *28*(18), 3505–3508, doi:10.1029/2001GL013194.

van der Hilst, R., R. Engdahl, W. Spakman, and G. Nolet (1991), Tomographic imaging of subducted lithosphere below northwest Pacific island arcs, *Nature*, *353*(6339), 37–43, doi:10.1038/353037a0.

Hong, T.-K., and H. Choi (2012), Seismological constraints on the collision belt between the North and South China blocks in the Yellow Sea, *Tectonophysics*, *570–571*, 102–113, doi:10.1016/j.tecto.2012.08.034.

Huang, J., and D. Zhao (2006), High-resolution mantle tomography of China and surrounding regions, *J. Geophys. Res. Solid Earth*, *111*(B9), B09305, doi:10.1029/2005JB004066.

Ita, J., and L. Stixrude (1992), Petrology, elasticity, and composition of the mantle transition zone, *J. Geophys. Res. Solid Earth*, *97*, 6849–6866, doi:10.1029/92jb00068.

Ito, E., and E. Takahashi (1989), Postspinel transformations in the system Mg2SiO4-Fe2SiO4 and some geophysical implications, *J. Geophys. Res. Solid Earth*, *94*(B8), 10637–10646, doi:10.1029/JB094iB08p10637.

Kee, W., S. Won Kim, Y. Jeong, and S. Kwon (2010), Characteristics of Jurassic Continental Arc Magmatism in South Korea: Tectonic Implications, *J. Geol.*,

118(3), 305–323, doi:10.1086/651503.

Kennett, B. L. N., and E. R. Engdahl (1991), Traveltimes for global earthquake location and phase identification, *Geophys. J. Int.*, *105*(2), 429–465, doi:10.1111/j.1365-246X.1991.tb06724.x.

Kim, Y., C. Lee, and S.-S. Kim (2015), Tectonics and volcanism in East Asia: Insights from geophysical observations, *J. Asian Earth Sci.*, *113, Part 2*, 842–856, doi:10.1016/j.jseaes.2015.07.032.

Kind, R., X. Yuan, and P. Kumar (2012), Seismic receiver functions and the lithosphere–asthenosphere boundary, *Tectonophysics*, *536–537*(0), 25–43, doi:10.1016/j.tecto.2012.03.005.

Lee, S.-H., J. Rhie, Y. Park, and K.-H. Kim (2014), Topography of the 410 and 660 km discontinuities beneath the Korean Peninsula and southwestern Japan using teleseismic receiver functions, *J. Geophys. Res. Solid Earth*, *119*(9), 2014JB011149, doi:10.1002/2014JB011149.

Ligorria, J. P., and C. J. Ammon (1999), Iterative deconvolution and receiver-function estimation, *Bull. Seismol. Soc. Am.*, *89*, 1395–1400.

Li, J., X. Wang, X. Wang, and D. A. Yuen (2013a), P and SH velocity structure in the upper mantle beneath Northeast China: Evidence for a stagnant slab in hydrous mantle transition zone, *Earth Planet. Sci. Lett.*, *367*, 71–81, doi:10.1016/j.epsl.2013.02.026.

Li, Q., R. Gao, F. T. Wu, Y. Guan, Z. Ye, Q. Liu, H. Kuo-Chen, R. He, W. Li, and X. Shen (2013b), Seismic structure in the southeastern China using teleseismic receiver functions, *Tectonophysics*, *606*, 24–35, doi:10.1016/j.tecto.2013.06.033.

Litasov, K. D., E. Ohtani, A. Sano, A. Suzuki, and K. Funakoshi (2005), Wet subduction versus cold subduction, *Geophys. Res. Lett.*, *32*(13), L13312, doi:10.1029/2005GL022921.

Li, X., and X. Yuan (2003), Receiver functions in northeast China – implications for slab penetration into the lower mantle in northwest Pacific subduction zone, *Earth Planet. Sci. Lett.*, *216*(4), 679–691, doi:10.1016/S0012-821X(03)00555-7.

Li, X., S. V. Sobolev, R. Kind, X. Yuan, and C. Estabrook (2000), A detailed receiver function image of the upper mantle discontinuities in the Japan subduction zone, *Earth Planet. Sci. Lett.*, *183*(3–4), 527–541, doi:10.1016/S0012-821X(00)00294-6.

Matsumoto, T., Y. Ito, H. Matsubayashi, and S. Sekiguchi (2006), Spatial distribution of F-net moment tensors for the 2005 West Off Fukuoka Prefecture Earthquake determined by the extended method of the NIED F-net routine, *Earth Planets Space*, *58*, 63–67.

Ma, Y. (2013), YASEIS: Yet Another computer program to calculate synthetic

seismograms for a spherically multi-layered Earth model, in *EGU General Assembly Conference Abstracts*, vol. 15, p. 5596.

Mégnin, C., and B. Romanowicz (2000), The three-dimensional shear velocity structure of the mantle from the inversion of body, surface and higher-mode waveforms, *Geophys. J. Int.*, *143*, 709–728, doi:10.1046/j.1365-246X.2000.00298.x.

Miller, M. S., and B. L. N. Kennett (2006), Evolution of mantle structure beneath the northwest Pacific: Evidence from seismic tomography and paleogeographic reconstructions, *Tectonics*, *25*(4), TC4002, doi:10.1029/2005TC001909.

Morishima, H., T. Kato, M. Suto, E. Ohtani, S. Urakawa, W. Utsumi, O. Shimomura, and T. Kikegawa (1994), The phase boundary between α- and β-Mg2SiO4 determined by in situ X-ray observation, *Science*, *265*(5176), 1202–1203, doi:10.1126/science.265.5176.1202.

Niu, F., A. Levander, S. Ham, and M. Obayashi (2005), Mapping the subducting Pacific slab beneath southwest Japan with Hi-net receiver functions, *Earth Planet. Sci. Lett.*, *239*(1–2), 9–17, doi:10.1016/j.epsl.2005.08.009.

Obayashi, M., H. Sugioka, J. Yoshimitsu, and Y. Fukao (2006), High temperature anomalies oceanward of subducting slabs at the 410-km discontinuity, *Earth Planet. Sci. Lett.*, *243*(1–2), 149–158, doi:10.1016/j.epsl.2005.12.032.

Obayashi, M., J. Yoshimitsu, and Y. Fukao (2009), Tearing of stagnant slab, *Science*, *324*(5931), 1173–1175, doi:10.1126/science.1172496.

Oh, C. W., T. Imayama, S. Y. Lee, S.-B. Yi, K. Yi, and B. C. Lee (2015), Permo-Triassic and Paleoproterozoic metamorphism related to continental collision in Yangpyeong, South Korea, *Lithos*, *216–217*, 264–284, doi:10.1016/j.lithos.2014.12.016.

Owens, T. J., A. A. Nyblade, H. Gurrola, and C. A. Langston (2000), Mantle transition zone structure beneath Tanzania, East Africa, *Geophys. Res. Lett.*, *27*, 827–830, doi:10.1029/1999gl005429.

Pandey, S., X. Yuan, E. Debayle, K. Priestley, R. Kind, F. Tilmann, and X. Li (2014), A 3D shear-wave velocity model of the upper mantle beneath China and the surrounding areas, *Tectonophysics*, *633*, 193–210, doi:10.1016/j.tecto.2014.07.011.

Park, Y., S.-C. Park, K.-H. Kim, M. Park, and J. Lee (2010), Magnitude scaling relationships from the first 3 s of P-wave arrivals in South Korea, *J. Seismol.*, *14*(4), 761–768, doi:10.1007/s10950-010-9198-3.

Ringwood, A. E. (1975), *Composition and petrology of the earth's mantle*, McGraw-Hill, New York.

Ringwood, A. E. (1994), Role of the transition zone and 660 km discontinuity in mantle dynamics, *Phys. Earth Planet. Inter.*, *86*(1–3), 5–24, doi:10.1016/0031-9201(94)05058-9.

Schmerr, N. (2012), The Gutenberg Discontinuity: Melt at the Lithosphere-Asthenosphere Boundary, *Science*, *335*(6075), 1480–1483, doi:10.1126/science.1215433.

Schmerr, N., and E. J. Garnero (2007), Upper mantle discontinuity topography from thermal and chemical heterogeneity, *Science*, *318*(5850), 623–626, doi:10.1126/science.1145962.

Seno, T., S. Stein, and A. E. Gripp (1993), A model for the motion of the Philippine Sea Plate consistent with NUVEL-1 and geological data, *J. Geophys. Res. Solid Earth*, *98*(B10), 17941–17948, doi:10.1029/93JB00782.

Seton, M., N. Flament, J. Whittaker, R. D. Müller, M. Gurnis, and D. J. Bower (2015), Ridge subduction sparked reorganization of the Pacific plate-mantle system 60–50 million years ago, *Geophys. Res. Lett.*, *42*(6), 2015GL063057, doi:10.1002/2015GL063057.

Shearer, P. M. (1996), Transition zone velocity gradients and the 520-km discontinuity, *J. Geophys. Res. Solid Earth*, *101*(B2), 3053–3066, doi:10.1029/95JB02812.

Shearer, P. M., and T. G. Masters (1992), Global mapping of topography on the 660-km discontinuity, *Nature*, *355*(6363), 791–796, doi:10.1038/355791a0.

Shin, Y. H., K. S. Choi, J.-S. Koh, S.-H. Yun, E. Nakamura, and S.-H. Na (2012), Lithospheric-folding-based understanding on the origin of the back-arc basaltic magmatism beneath Jeju volcanic island: LITHOSPHERIC-FOLDING-BASED MAGMATISM, *Tectonics*, *31*(4), n/a–n/a, doi:10.1029/2011TC003092.

Shito, A., and T. Shibutani (2001), Upper mantle transition zone structure beneath the Philippine Sea Region, *Geophys. Res. Lett.*, *28*(5), 871–874, doi:10.1029/2000GL012235.

Simmons, N. A., and H. Gurrola (2000), Multiple seismic discontinuities near the base of the transition zone in the Earth's mantle, *Nature*, *405*, 559–562.

Sodoudi, F., X. Yuan, Q. Liu, R. Kind, and J. Chen (2006), Lithospheric thickness beneath the Dabie Shan, central eastern China from S receiver functions, *Geophys. J. Int.*, *166*(3), 1363–1367, doi:10.1111/j.1365-246X.2006.03080.x.

Song, T.-R. A., D. V. Helmberger, and S. P. Grand (2004), Low-velocity zone atop the 410-km seismic discontinuity in the northwestern United States, *Nature*, *427*(6974), 530–533, doi:10.1038/nature02231.

Suetsugu, D., T. Inoue, A. Yamada, D. Zhao, and M. Obayashi (2006), Towards mapping the three-dimensional distribution of water in the transition zone from P-velocity tomography and 660-km discontinuity depths, in *Geophysical Monograph Series*, vol. 168, edited by S. D. Jacobsen and S. van der Lee, pp. 237–249, American Geophysical Union, Washington, D. C.

Suetsugu, D. et al. (2010), Depths of the 410-km and 660-km discontinuities in and around the stagnant slab beneath the Philippine Sea: Is water stored in the

stagnant slab?, *Phys. Earth Planet. Inter.*, *183*(1–2), 270–279, doi:10.1016/j.pepi.2010.09.004.

Tajima, F., I. Katayama, and T. Nakagawa (2009), Variable seismic structure near the 660 km discontinuity associated with stagnant slabs and geochemical implications, *Phys. Earth Planet. Inter.*, *172*(3–4), 183–198, doi:10.1016/j.pepi.2008.09.013.

Tang, Y.-J., H.-F. Zhang, M. Santosh, and J.-F. Ying (2013), Differential destruction of the North China Craton: A tectonic perspective, *J. Asian Earth Sci.*, *78*, 71–82, doi:10.1016/j.jseaes.2012.11.047.

Tauzin, B., R. D. van der Hilst, G. Wittlinger, and Y. Ricard (2013), Multiple transition zone seismic discontinuities and low velocity layers below western United States, *J. Geophys. Res. Solid Earth*, *118*(5), 2307–2322, doi:10.1002/jgrb.50182.

Tian, X., J. Teng, H. Zhang, Z. Zhang, Y. Zhang, H. Yang, and K. Zhang (2011), Structure of crust and upper mantle beneath the Ordos Block and the Yinshan Mountains revealed by receiver function analysis, *Phys. Earth Planet. Inter.*, *184*(3–4), 186–193, doi:10.1016/j.pepi.2010.11.007.

Tonegawa, T., K. Hirahara, and T. Shibutani (2005), Detailed structure of the upper mantle discontinuities around the Japan subduction zone imaged by receiver function analyses, *Earth Planets Space*, *57*(1), 5–14.

Tono, Y., T. Kunugi, Y. Fukao, S. Tsuboi, K. Kanjo, and K. Kasahara (2005), Mapping of the 410- and 660-km discontinuities beneath the Japanese islands, *J. Geophys. Res. Solid Earth*, *110*(B3), B03307, doi:10.1029/2004JB003266.

Tseng, T.-L., and W.-P. Chen (2004), Contrasts in seismic wave speeds and density across the 660-km discontinuity beneath the Philippine and the Japan Seas, *J. Geophys. Res. Solid Earth*, *109*(B4), B04302, doi:10.1029/2003JB002613.

Whittaker, J. M., R. D. Müller, and M. Sdrolias (2007), Revised history of Izanagi-Pacific ridge subduction, p. 96, Honolulu, Hawaii.

Wu, F.-Y., J.-Q. Lin, S. A. Wilde, X. Zhang, and J.-H. Yang (2005), Nature and significance of the Early Cretaceous giant igneous event in eastern China, *Earth Planet. Sci. Lett.*, *233*(1–2), 103–119, doi:10.1016/j.epsl.2005.02.019.

Xu, X., S. Y. O'reilly, W. L. Griffin, and X. Zhou (2000), Genesis of Young Lithospheric Mantle in Southeastern China: an LAM–ICPMS Trace Element Study, *J. Petrol.*, *41*(1), 111–148, doi:10.1093/petrology/41.1.111.

Xu, Y.-G. (2007), Diachronous lithospheric thinning of the North China Craton and formation of the Daxin'anling–Taihangshan gravity lineament, *Lithos*, *96*(1–2), 281–298, doi:10.1016/j.lithos.2006.09.013.

Yamada, A., D. Zhao, T. Inoue, D. Suetsugu, and M. Obayashi (2009), Seismological evidence for compositional variations at the base of the mantle transition zone under Japan Islands, *Gondwana Res.*, *16*(3–4), 482–490,

doi:10.1016/j.gr.2009.04.009.

Yoo, H. J., R. B. Herrmann, K. H. Cho, and K. Lee (2007), Imaging the Three-Dimensional Crust of the Korean Peninsula by Joint Inversion of Surface-Wave Dispersion and Teleseismic Receiver Functions, *Bull. Seismol. Soc. Am.*, *97*(3), 1002–1011, doi:10.1785/0120060134.

Zhao, D. (2004), Global tomographic images of mantle plumes and subducting slabs: insight into deep Earth dynamics, *Phys. Earth Planet. Inter.*, *146*(1–2), 3–34, doi:10.1016/j.pepi.2003.07.032.

Zhao, D., Y. Yamamoto, and T. Yanada (2013), Global mantle heterogeneity and its influence on teleseismic regional tomography, *Gondwana Res.*, *23*(2), 595–616, doi:10.1016/j.gr.2012.08.004.

Zhao, W. et al. (2011), Tibetan plate overriding the Asian plate in central and northern Tibet, *Nat. Geosci.*, *4*(12), 870–873, doi:10.1038/ngeo1309.

Zhu, R.-X., J.-H. Yang, and F.-Y. Wu (2012), Timing of destruction of the North China Craton, *Lithos*, *149*, 51–60, doi:10.1016/j.lithos.2012.05.013.

초록

원격수신함수의 CCP 합산 방법을 사용한 한반도 주변 지역의 상부 맨틀 불연속면에 관한 연구

이상현
지진학, 지구물리학
지구환경과학부
서울대학교 대학원

원격수신함수를 사용하여 한반도와 일본 동남부 지역 하부의 상부맨틀 불연속면(410 불연속면과 660 불연속면)의 깊이변화를 살펴보았다. 획득된 수신함수는 일차원 속도구조와 삼차원 속도구조에 대하여 계산된 각 깊이에서 P-to-s 변환된 위치와 도달시간차이에 의하여 삼차원 공간으로 마이그레이션된 후, common conversion point (CCP) 합산법이 적용되었다. CCP 합산된 수신함수들은 전체 연구지역에서양의 값을 가지는 410 불연속면과 660 불연속면을 보여주고 있다. 전반적으로 불연속면의 깊이 변화는 섭입하는 차가운 태평양판의 분포와 부합하는 결과를 보여준다. 하지만, 자세히 살펴보면 섭입판의 차가운 온도만으로 설명할 수 없는 불연속면의 깊이 변화가 관측되었으며, 이는 섭입판의 복잡한 구조에서 기인한 것으로 사료된다. 한반도와 규슈지역에서 관측된 침강된 410 불연속면은 트렌치의 후퇴 작용과 관련된 구조로 사료된다. 660 불연속면은 위도에 따라 매우 다른 특성을 보이고 있다. 위도 38° N 북쪽에서는 남쪽에서와는 달리 차가운 섭입판의 존재에도 불구하고 깊이의 변화가

미약하게 나타났다. 이러한 차이는 Japan Trench 와 Izu-Bonin Trench 에서의 섭입각의 차이에 의한 나타난 결과일 가능성이 있다. 또한, 두 지역의 물 함량에 큰 차이가 있어 생긴 결과일 수 있다.

S 파 수신함수를 사용하여 한반도 하부의 LAB(암석권-연약권 경계)의 깊이를 구하였다. 각 수신함수는 IASP91 모델을 가정하여 도달 시간 차이로부터 계산된 S-to-p 변환 위치로 마이그레이션하였다. CCP 합산법에 의하여 한반도 하부에서 저속도층의 경계를 이미징하였다. 한반도 하부에서 LAB 는 약 60 – 100 km 깊이에 위치하는 것으로 나타났다. 이는 한반도가 선캄브리아 시대에 생성된 대륙임을 고려할 때 예상되는 것에 비하여 매우 작은 값으로, 쥬라기 시대에 고태평양판이 섭입하면서 lithosphere thinning 이 발생하였음을 시사하고 있다. 지역적으로 경기 육괴와 옥천대의 경계에서 LAB 의 깊이가 크게 변하는 것이 관측되었다. 북쪽 지역에서는 LAB 의 깊이가 깊게 나타나며, 남쪽에서는 얕게 나타난다. 또한 남쪽에서는 LAB 하부에 또 다른 저속도층의 존재가 발견되었다. 기존에 제시된 여러 텍토닉 모델들은 이러한 한반도의 LAB 구조와 화성활동을 동시에 설명할 수 없었다. 한반도의 LAB 구조는 다양한 분야에서 추후 한반도의 형성 과정을 이해하는 데 큰 도움이 될 것으로 기대된다.

주요어 : 원격수신함수, CCP 합산법, 한반도, 410 불연속면, 660 불연속면, LAB

학번 : 2002-20598